Int. J. Therm. Sci. (1999) 38, 5–26

Melting driven by natural convection
A comparison exercise: first results[1]

Olivier Bertrand[a], Bruno Binet[b], Hervé Combeau[c], Stéphane Couturier[d], Yves Delannoy[e], Dominique Gobin[f]*, Marcel Lacroix[b], Patrick Le Quéré[g], Marc Médale[h], Jure Mencinger[i], Hamou Sadat[d], Gisele Vieira[f]

[a] *Master-ENSCPB, BP 108, 33402 Talence cedex, France*
[b] *Thermaus, Université de Sherbrooke, Sherbrooke, Québec, J1K 2R1, Canada*
[c] *LSGMM, École des mines de Nancy, Parc de Saurupt, 54042 Nancy, France*
[d] *LET, UMR CNRS 6608, Ensma, 86960, Futuroscope Cedex, France*
[e] *EMP/Madylam, BP 95, 38402 St-Martin-d'Hères cedex, France*
[f] *Fast, UMR CNRS 7608, Campus universitaire, Bât. 502, 91405 Orsay, France*
[g] *Limsi, BP 133, 91403 Orsay cedex, France*
[h] *Iusti, UMR CNRS 6595, Technopôle de Château-Gombert, 13453 Marseille cedex 13, France*
[i] *LFDT, University of Ljubljana, Aškerčeva 6, 1000 Ljubljana, Slovenia*

(Received 8 July 1998, accepted 8 october 1998)

Abstract—This paper presents the first results of a benchmark problem concerning the simulation of coupled natural convection and melting from an isothermal vertical wall. The exercise is restricted to the simulation of phase change of pure substances, driven by laminar natural convection in 2D enclosures. The comparison covers two ranges of Prandtl numbers, corresponding to the melting of metals or organic materials. The results of the test cases are presented in detail and show that, while qualitative agreement is obtained in most situations, it is still relevant to proceed to thorough numerical comparisons before assessing the accuracy of the different algorithms. The dispersion of the results is a strong motivation to extend the exercise to a second stage incorporating a larger number of contributions. © Elsevier, Paris

phase change / natural convection / moving boundaries / conjugate heat transfer / benchmark

Résumé — Fusion contrôlée par convection naturelle. Un exercice de comparaison : premiers résultats. Cet article présente les premiers résultats d'un banc d'essais numérique consacré à la simulation de la fusion couplée à la convection naturelle le long d'une paroi verticale isotherme. L'exercice est limité au cas des substances pures et de la convection laminaire en cavité bidimensionnelle. La comparaison porte sur deux domaines de nombres de Prandtl, correspondant à des matériaux métalliques ou organiques. Les résultats des tests sont détaillés et montrent que, si on parvient à un accord qualitatif dans la plupart des cas, il reste pertinent de procéder à des comparaisons rigoureuses avant d'établir la précision des différents algorithmes. La dispersion des résultats conduit à proposer une seconde étape à cette comparaison et à l'étendre à un plus grand nombre de contributions. © Elsevier, Paris

changement de phase / convection naturelle / frontière mobile / transferts couplés / banc d'essai

Nomenclature

A	aspect ratio of the enclosure, $= H/L$	
C_P	specific heat of the liquid phase	$\mathrm{J{\cdot}kg^{-1}{\cdot}K^{-1}}$
Fo	Fourier number, $= \alpha\, t^*/H^2$	
g	acceleration of gravity	$\mathrm{m{\cdot}s^{-2}}$
Gr	Grashof number, $= g\,\beta\,\Delta T\, H^3/\nu^2$	
H	height of the enclosure	m
$\vec{k}$	unit vector in the vertical direction	
k	thermal conductivity of the liquid	$\mathrm{W{\cdot}m^{-1}{\cdot}K^{-1}}$
L	width of the enclosure	m
L_F	latent heat	$\mathrm{J{\cdot}kg^{-1}}$
Nu	average Nusselt number	

[1] This synthesis was written by D. Gobin and P. Le Quéré.
* Correspondance et tirés à part.

P	dimensionless pressure	
Pr	Prandtl number, $= \nu/\alpha$	
Ra	Rayleigh number, $= Pr\, Gr$	
Ste	Stefan number, $= C_P(T_1 - T_F)/L_F$	
t^*	dimensional time	s
T	dimensional temperature	°C
T_F	melting temperature	°C
T_0	initial temperature	°C
T_1	hot wall temperature	°C
$\vec{V}$	dimensionless fluid velocity, $= \vec{v^*}\, H/\nu$	
$w(u)$	vertical (horizontal) component of $\vec{V}$	
$x(z)$	dimensionless coordinates, $= x^*/H$ (z^*/H)	

Greek symbols

α	thermal diffusivity	$m^2 \cdot s^{-1}$
β	coefficient of volumetric thermal expansion	$°C^{-1}$
ΔT	temperature difference between walls, $T_1 - T_F$	°C
ν	kinematic viscosity	$m^2 \cdot s^{-1}$
ρ	fluid density	$kg \cdot m^{-3}$
τ	dimensionless time, $= Fo \times Ste$	
θ	dimensionless temperature, $= (T - T_0)/\Delta T$	

1. INTRODUCTION

Solid liquid phase changes occur in many industrial or natural processes and their understanding, modelisation and numerical simulation has thus motivated a large number of analytical, experimental and numerical studies over the last 30 years. Nowadays, due to the increasing need for reliable numerical simulations of industrial or technological processes, and as a result of increasing computational capabilities, more and more complex problems are being tackled in various research areas, accounting for the interaction between phase change and fluid flow, heat and species transfer in multicomponent systems, and solidification models including columnar 'mushy' zones and transport of equiaxed grains [1, 2].

In this context, our interest is to propose a numerical exercise comparing different physical models and numerical procedures on a relatively simpler problem, where phase change (here melting) is driven by laminar thermal convection in the melt. A large number of papers related to this problem may be found in the litterature, but few studies have been dedicated to a systematical comparison of independent numerical algorithms. First attempts are due to Lacroix and Voller [3] and then to Viswanath and Jaluria [4]: in both cases the purpose of the exercise is to compare a front-tracking or transformed grid procedure to a fixed grid or enthalpy method (see also the review by Voller [5]). The test problem refers essentially to the experimental situation presented by Gau and Viskanta [6] for the melting of gallium: only the low Pr number range characterising liquid metals ($Pr \approx 10^{-2}$) is studied.

On the other hand, comparisons of numerical computations with experimental results have been reported in the litterature [7–11]. Although global qualitative agreement is generally found, detailed quantitative comparisons have been generally in conclusive due to the fact that many difficulties are met when trying to satisfy experimentally a number of hypotheses or approximations accepted by the numerical codes. Adiabatic horizontal walls, instantaneous temperature increase at the hot wall, or negligible density differences between the solid and liquid phase are rarely obtained in the experiments. Significant differences may even be found between independent experiments, depending on the measurement techniques used to scan the melting front position, as shown by Campbell and Koster [12].

It is thus still out of reach to provide reference experiments which could be used for the purpose of assessing the validity of numerical simulation procedures. The present comparison exercise is thus intended to provide a common framework and sets of results in order to analyse in detail the characteristics of the numerical solutions in 2D natural convection dominated melting processes, over a wide range of governing parameters. This presentation is a first synthesis based on a small number of contributions, with the intention of assessing the relevance of the exercise. A second, more inclusive step in this comparison is to be organized in the next few months and the present conclusions are obviously provisional.

2. DESCRIPTION

2.1. Problem Definition

The problem under consideration deals with melting of a pure substance controlled by natural convection in the melt. One considers a 2D square cavity (height H = width L) initially filled with a solid material at a uniform temperature ($T_0 = T_F$). At $t^* = 0$, the temperature of one of the vertical walls (the left wall in *figure 1*) is raised to a value $T_1 > T_F$, while the other vertical wall is maintained at the initial temperature. The horizontal walls are assumed to be adiabatic and no-slip. The fluid flow is supposed to be in the laminar regime, and the thermophysical properties of the material constant.

After a pure conduction stage, thermal convection develops in the liquid phase, causing a non-uniform distribution of the heat flux at the interface and a non-uniform displacement of the melting front.

2.2. Proposed test cases

The problem is characterised by the Prandtl and Rayleigh numbers, the Stefan number and the global

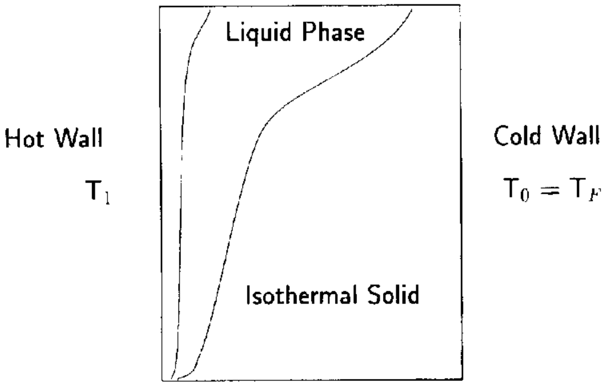

Figure 1. Schematic diagram of the problem.

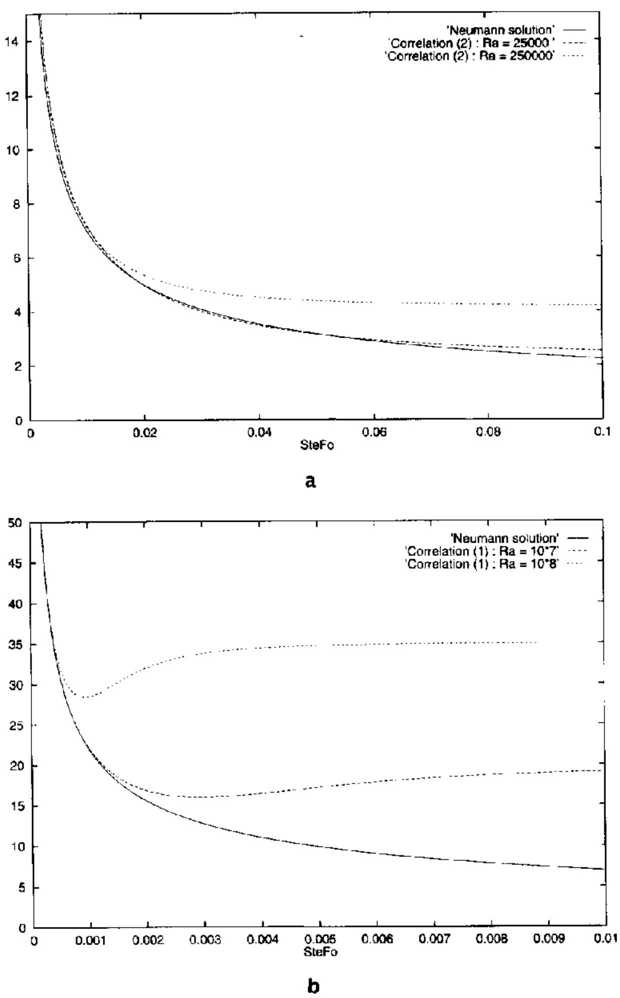

Figure 2. Correlations for the average Nusselt number evolution. **a)** Nusselt number at the vertical wall: $Pr = 0.02$, $Ste = 0.01$ (equation (2)). **b)** Nusselt number at the vertical wall: $Pr = 50$, $Ste = 0.1$ (equation (1)).

aspect ratio of the enclosure. Two groups of numerical tests have been proposed, corresponding to distinct ranges of the liquid phase Prandtl number: the *low* Prandtl number range ($Pr \sim 10^{-2}$, melting of metals) and the *high* Prandtl number range ($Pr \sim 10^{2}$, melting of paraffin waxes).

The governing parameters have been estimated using approximate values of the thermophysical properties of tin and octadecane (*table I*). For a given geometry ($A = 1$), the values of the Rayleigh and Stefan numbers correspond to a dimensional height of the enclosure $H = 0.10$ m and a reference temperature difference $T_1 - T_F = 3$ °C for tin (Case 2) and 10 °C for octadecane (Case 4), leading to the values displayed in *table II*. In each Pr range, a 10 times smaller Rayleigh number (Cases 1 and 3) is also considered.

In order to limit the outputs, the following results are specified:

(1) the time evolution of the melted volume and of the average Nusselt number at the hot wall;

TABLE I
Thermophysical properties considered in the definition of the test cases.

Property or parameter	Low Prandtl number (Tin)	High Prandtl number (Octadecane)
k ($W \cdot mK^{-1}$)	60	0.2
C_P ($J \cdot kg \cdot K^{-1}$)	200	1 250
ρ ($kg \cdot m^{-3}$)	7 500	800
α ($m^2 \cdot s^{-1}$)	$4 \cdot 10^{-5}$	$2 \cdot 10^{-7}$
ν ($m^2 \cdot s^{-1}$)	$8 \cdot 10^{-7}$	10^{-5}
Pr	0.02	50
L_F ($J \cdot kg^{-1}$)	$6 \cdot 10^4$	$1.25 \cdot 10^5$
T_F (°C)	232	30
ΔT (°C)	3	10
Ste	0.01	0.1
β (K^{-1})	$8/3 \cdot 10^{-4}$	$2 \cdot 10^{-3}$
$H = L$ (m)	0.10	0.10
g ($m \cdot s^{-2}$)	10	10
Gr	$1.25 \cdot 10^7$	$2 \cdot 10^6$
Ra	$2.5 \cdot 10^5$	10^8

TABLE II
Test cases: parameters.

$Pr = 0.02$ $Ste = 0.01$	$Ra = 2.5 \cdot 10^4$ Case 1	$Ra = 2.5 \cdot 10^5$ Case 2
$Pr = 50$ $Ste = 0.1$	$Ra = 10^7$ Case 3	$Ra = 10^8$ Case 4

(2) the position of the melting front and the local Nusselt number distribution at four different times (expressed in the dimensionless form $\tau = Fo\,Ste = \alpha t^* Ste/H^2$:

at $Pr = 0.02$: $t_1 = 4{\cdot}10^{-3}$, $t_2 = 10^{-2}$, $t_3 = 4{\cdot}10^{-2}$ and $t_4 = 10^{-1}$,

– at $Pr = 50$: $t_1 = 5{\cdot}10^{-4}$, $t_2 = 2{\cdot}10^{-3}$, $t_3 = 6{\cdot}10^{-3}$ and $t_4 = 10^{-2}$.

3. HEAT TRANSFER CORRELATIONS

Early studies concerning the characteristic scales of the problem have been performed by Webb and Viskanta [13] and Beckermann and Viskanta [14]. A more complete description of the problem and an analysis of the relevant parameters and of the scaling laws may be found in the paper by Jany and Bejan [15]. The main features are described in this section.

In the first stage of the melting process, pure conduction is the dominating heat transfer mechanism. The interface moves parallel to the hot wall, and the time evolution of the front position is given by the classical solution of the Stefan problem ($s(t) \sim \sqrt{t}$ [16]). Accordingly the Nusselt number decreases like $1/\sqrt{t}$. Then, as the thickness of the liquid layer grows with time, the influence of convection on heat transfer is felt in the top part of the enclosure and progressively along the whole interface. In this transition regime, the competition between pure conduction and natural convection limits the Nusselt number decrease, which goes through a minimum, and then increases when the heat transfer regime is dominated by convection. Finally the boundary layers in the liquid separate, and the average heat transfer reaches a constant value.

This analysis was carried out in the high Pr number range, and Jany and Bejan [15] show that the different time scales and heat transfer rates are readily expressed in terms of power laws of the Rayleigh number. The same approach may be extended to the range of low Pr numbers, where the relevant governing parameter is shown to be the dimensionless group $Ra \times Pr$.

The scaling laws lead to correlations for the evolution of the average Nusselt number as a function of time ($\tau = Fo\,Ste$); the value of the coefficients are identified from the results of numerical simulations.

1) In the range $Pr \geq 1$:

$$Nu(\tau) = \frac{1}{\sqrt{2\tau}} + \frac{Nu_\infty - 1/\sqrt{2\,\tau}}{\sqrt{1 + \dfrac{1}{(0.0175\,Ra^{3/4}\,\tau^{3/2})^2}}}. \qquad (1)$$

2) In the range $Pr << 1$:

$$Nu(\tau) = Nu_\infty + \frac{1}{\sqrt{2\,\tau}}\left[1 - \frac{1}{\sqrt{1 + \dfrac{1}{((Ra\,Pr)^{0.36}\tau^{0.75})^2}}}\right] \qquad (2)$$

Where Nu_∞ is given by the expressions $Nu_\infty = 0.33\,Ra^{0.25}$ in the $Pr >> 1$ range according to Bénard et al. [7], and $Nu_\infty = 0.29\,Ra^{0.27}\,Pr^{0.18}$ in the $Pr << 1$ range [10], or by the more general correlation proposed by Lim and Bejan [17] for any value of Pr:

$$Nu_\infty = \frac{0.35\,Ra^{1/4}}{[1 - (0.143/Pr)^{9/16}]^{4/9}}. \qquad (3)$$

4. PRESENTATION OF THE RESULTS

Contributions to this first stage of the benchmark have been requested within the framework of a project shaved among a network of French research laboratories concerned with the simulation of heat and mass transfer processes (Ameth). The participants are listed in *table III.* Brief descriptions of the different methods and numerical procedures used for the solution of the problem are given in the appendix.

In the following sections, the results are compared in *figures 3* to *10.* For each case, three outputs are displayed and compared:

(1) the time evolution of the average Nusselt number at the hot wall obtained by the contributors, compared to the Neumann solution and to the existing correlation recalled in section 3;

TABLE III
Contributions to the present benchmark.

Author	Laboratory	Cas
M. Lacroix	Thermaus-Sherbrooke	1–2–3–4
G. Vieira D. Gobin	Fast–Orsay	2–3–4
B. Binet M. Lacroix	Thermaus-Sherbrooke	1–2–3–4
M. Médale	Iusti–Marseille	2
O. Bertrand E. Arquis	Master-Bordeaux	2
Y. Delannoy	EPM/Madylam Grenoble	3 4
S. Cousturier H. Sadat	LET–Poitiers	1–2–3
J. Mencinger B. Šarler	LFDT–Ljubljana	1–2
H. Combeau	LSGMM–Nancy	1–2
P. Le Quéré	LIMSI Orsay	1 2–3–4

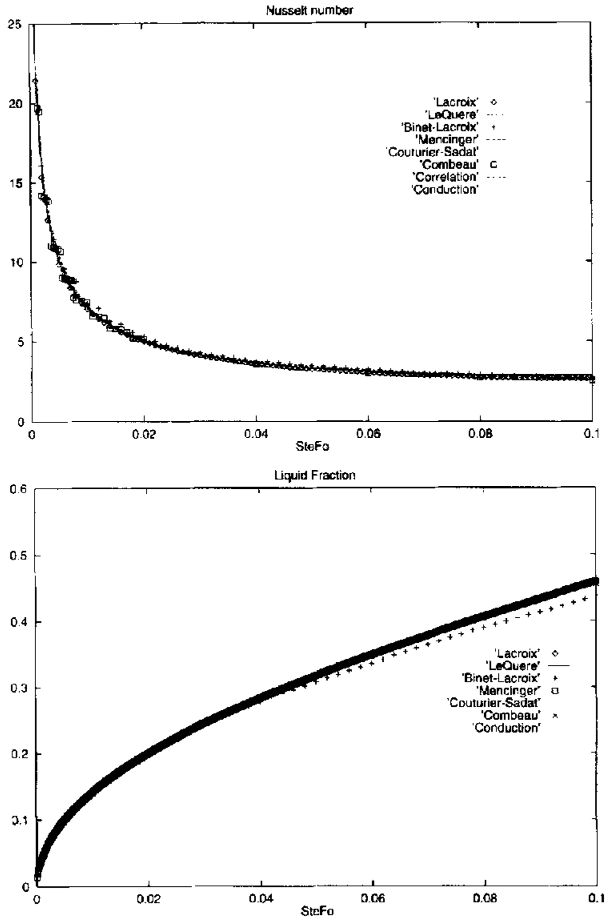

Figure 3. Comparison of the average values for case 1. $Pr = 0.02$, $Ste = 0.01$, $Ra = 2.5 \cdot 10^4$. **a)** Nusselt number at the vertical wall. **b)** Liquid fraction.

(2) the time evolution of the liquid fraction (the dimensionless melted volume);

(3) the position of the melting front at four different times of the process.

Among the 10 sets of results received, most contributions have used fixed grid or 'enthalpy' methods (FG), including a commercial software package (Fluent™: Delannoy) and two have used a front-tracking of the transformed grid procedure (TG). Six contributions have presented results for cases #1 and #3, eight for case #2 and five for case #4. Only three contributors have solved the four problems.

5. ANALYSIS OF THE RESULTS

Hereafter, the comparison is made separately in the two ranges of Pr number.

5.1. The low Prandtl number range (cases # 1 and #2)

Case # 1 was carried out by six participants, Lacroix, Binet–Lacroix, Mencinger, Couturier–Sadat, Combeau and Le Quéré. For this test case, all six simulations are in good agreement. No significant difference was noted for the Nusselt number, except for the solution by Binet (*figure 3*), which gives a slightly slower evolution of the melting front (about 4 %). On the melting front positions (*figure 4*) however, the solution by Combeau seems to be slightly slower that the average. As a general remark, the discrepancies between the different solutions are small (see *figure 11*), which is obviously due to the fact that at such a low Ra number, the convective transfer is very limited, and the evolution is very close to the pure conduction solution. In *figure 3*, the plot of the Neumann solution cannot be clearly distinguished from the computational results.

Case # 2 was carried out by eight participants, Lacroix, Gobin–Viera, Bertrand–Arquis, Binet–Lacroix, Mencinger, Couturier-Sadat, Combeau and Le Quéré[2]. In the test case, in spite of the relative uniformity of the results in terms of the average values (±5 % on the melted volume), the differences are more important regarding the local interface position. The positions at early times (t_1 and t_2) are almost uniformly identical, but at time t_4, significant differences may be noticed all along the interface, even in the bottom part of the enclosure. Also the position of the 'knee' corresponding to the main recirculation largely varies, typically presenting the same dispersion as the results reported in [4].

In the interface positions displayed at time t_3, two methods (Le Quéré and Couturier–Sadat) predict a quite different shape of the front, with a significantly larger interface velocity at mid-height of the enclosure. This is probably due to the fact that these two methods used a full transient procedure with small time steps which results in the prediction of two recirculating cells at this time of the evolution. As a consequence, the local heat transfer at the interface, and thus the local front velocity are modified. Actually the flow structure evolution given by this solution is even more complex, since a four cell structure is found at early times, evolving towards 3 and then 2 rolls after successive merging of the two upper cells. Also note on the enlargement of the Nusselt number (*figure 12*) that the flow structure predicted by Le Quéré is oscillatory, with high frequency oscillations developing on top of the slow time-scale evolution characteristic of the melting process. The appearance of multiple cell solutions found by Le Quéré and Couturier–Sadat is qualitatively consistent with the calculations by Dantzig [18] who also reported multiple

[2] Couturier-Sadat and Le Quéré carried out the simulation to t_3 only.

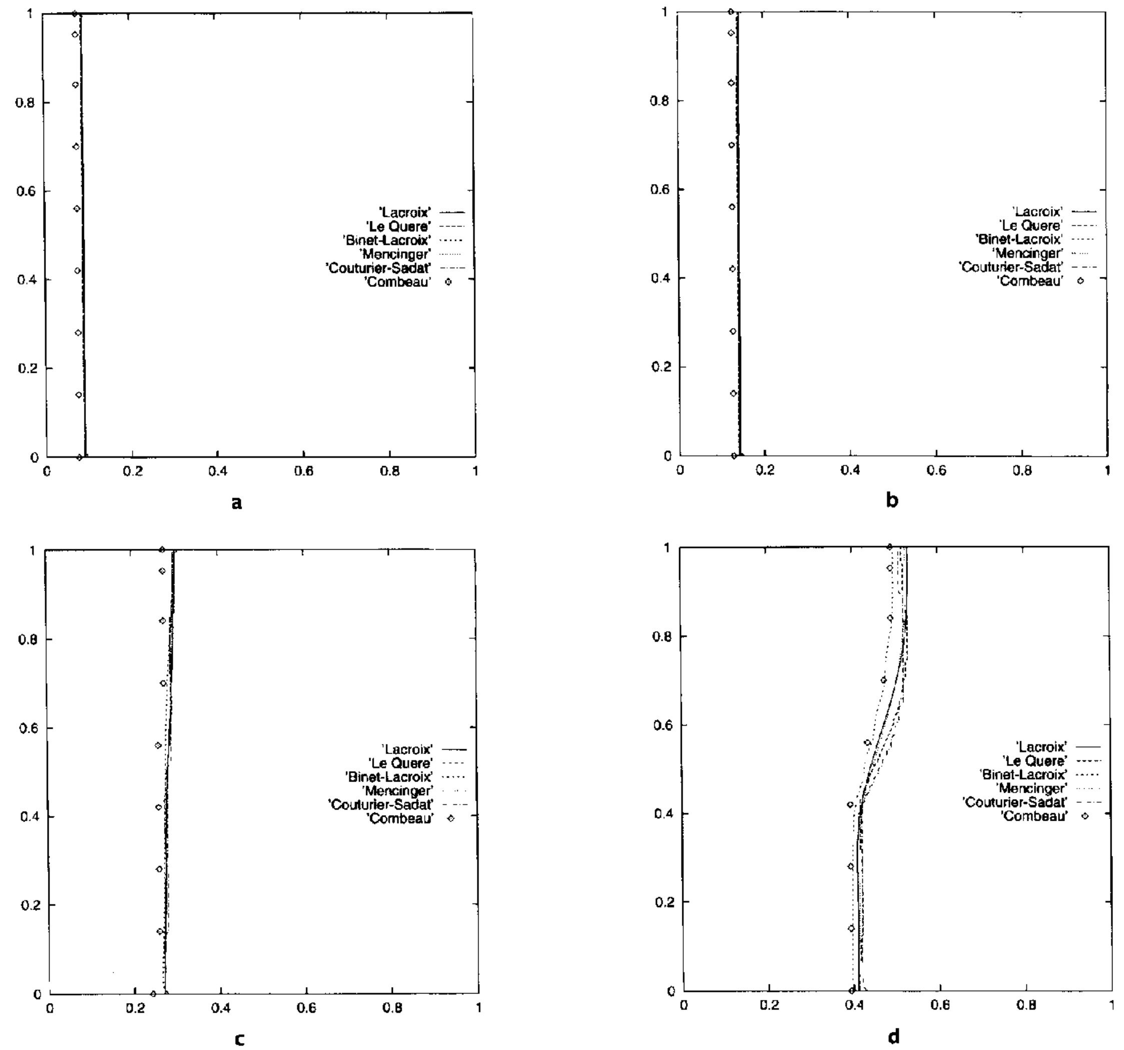

Figure 4. Case 1. Melting front positions. **a)** $Ste\,Fo = 0.004$, **b)** $Ste\,Fo = 0.01$, **c)** $Ste\,Fo = 0.04$, **d)** $Ste\,Fo = 0.10$.

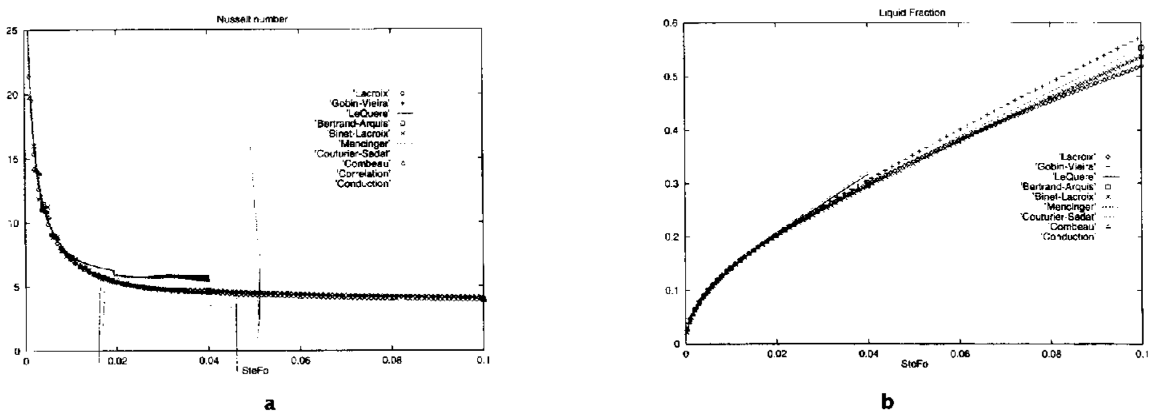

Figure 5. Comparison of the average values for case 2. $Pr = 0.02$, $Ste = 0.01$, $Ra = 2.5{\cdot}10^5$. **a)** Nusselt number at the vertical wall. **b)** Liquid fraction.

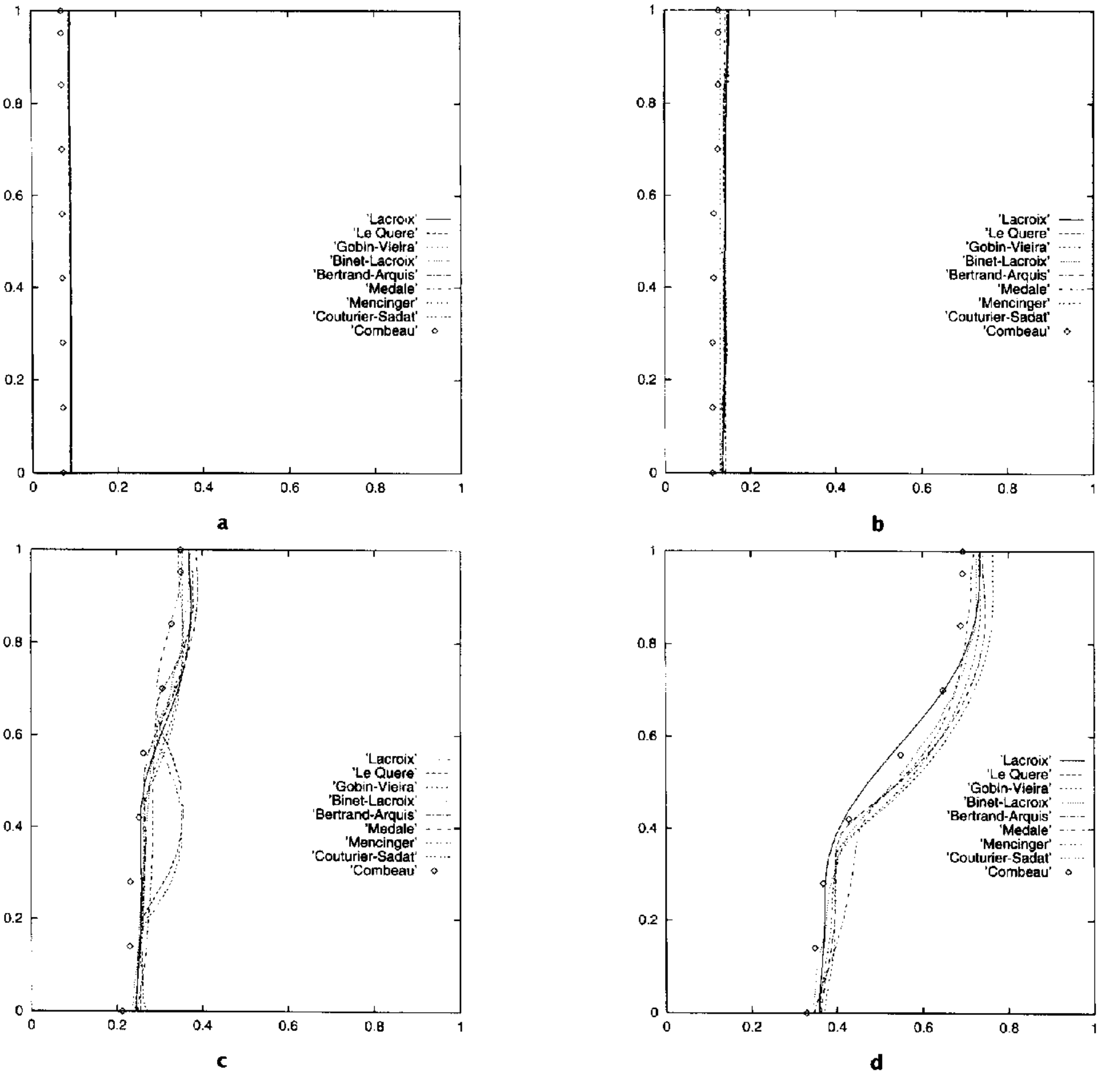

Figure 6. Case 2. Melting front positions. **a)** $Ste\,Fo = 0.004$. **b)** $Ste\,Fo = 0.01$, **c)** $Ste\,Fo = 0.04$. **d)** $Ste\,Fo = 0.10$.

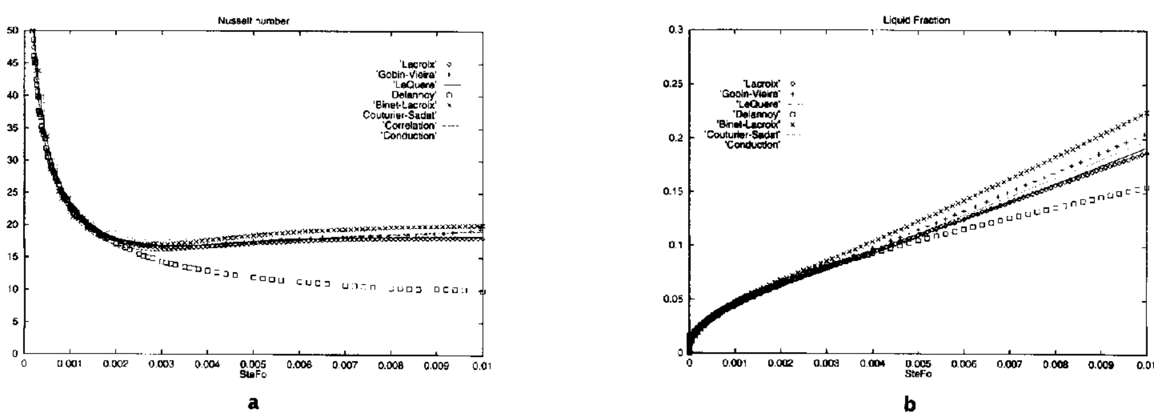

Figure 7. Comparison of the average values for case 3. $Pr = 50$. $Ste = 0.1$. $Ra = 10^7$. **a)** Nusselt number at the vertical wall. **b)** Liquid fraction.

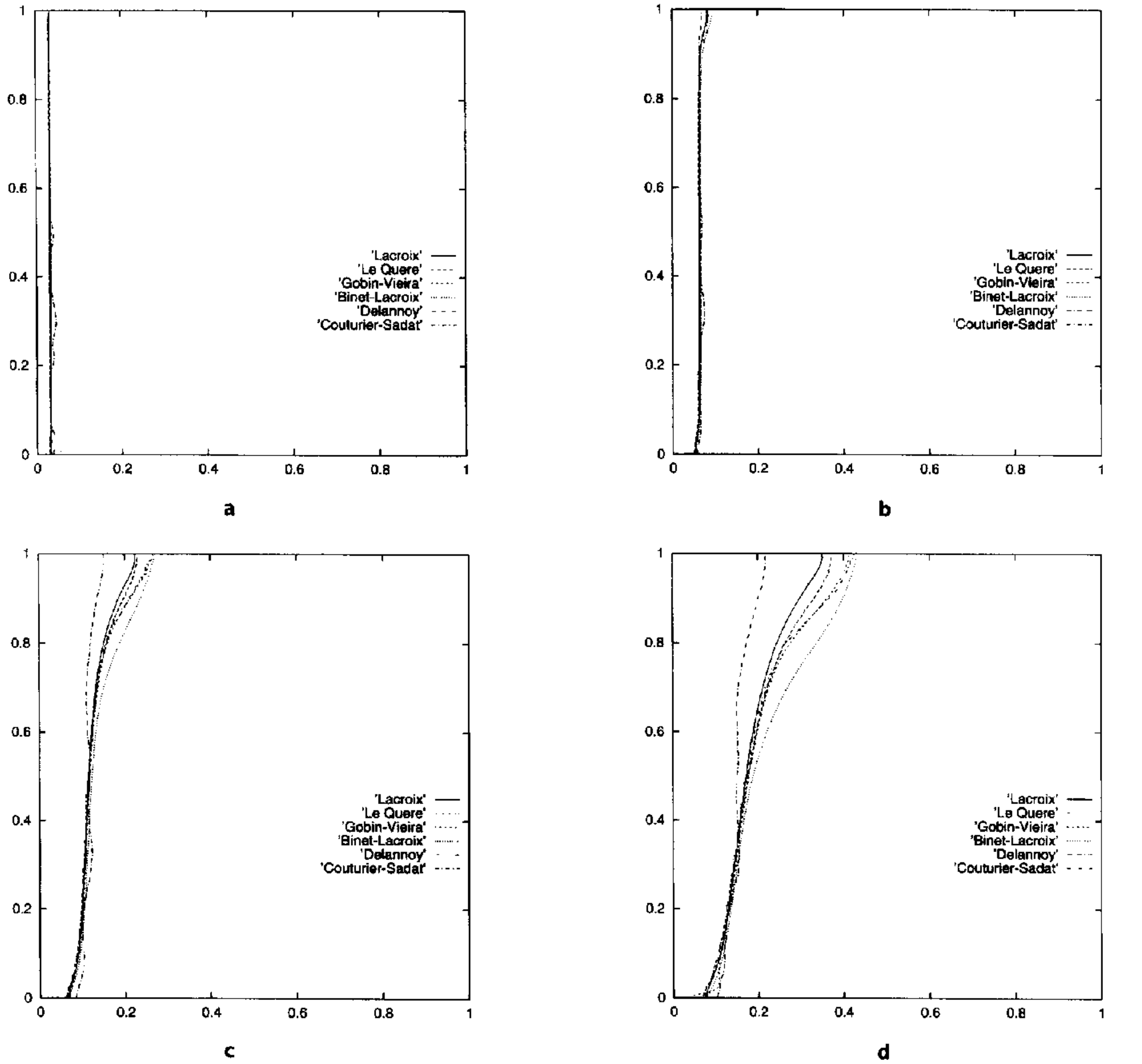

Figure 8. Case 3. Melting front positions. **a)** $Ste\,Fo = 0.0005$. **b)** $Ste\,Fo = 0.002$. **c)** $Ste\,Fo = 0.006$. **d)** $Ste\,Fo = 0.010$.

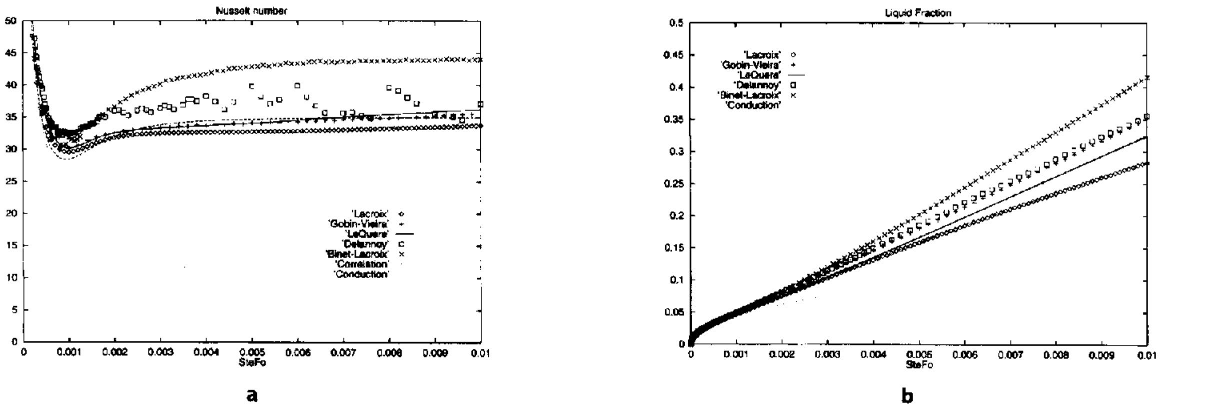

Figure 9. Comparison of the average values for case 4. $Pr = 50$. $Ste = 0.1$. $Ra = 10^8$. **a)** Nusselt number at the vertical wall. **b)** Liquid fraction.

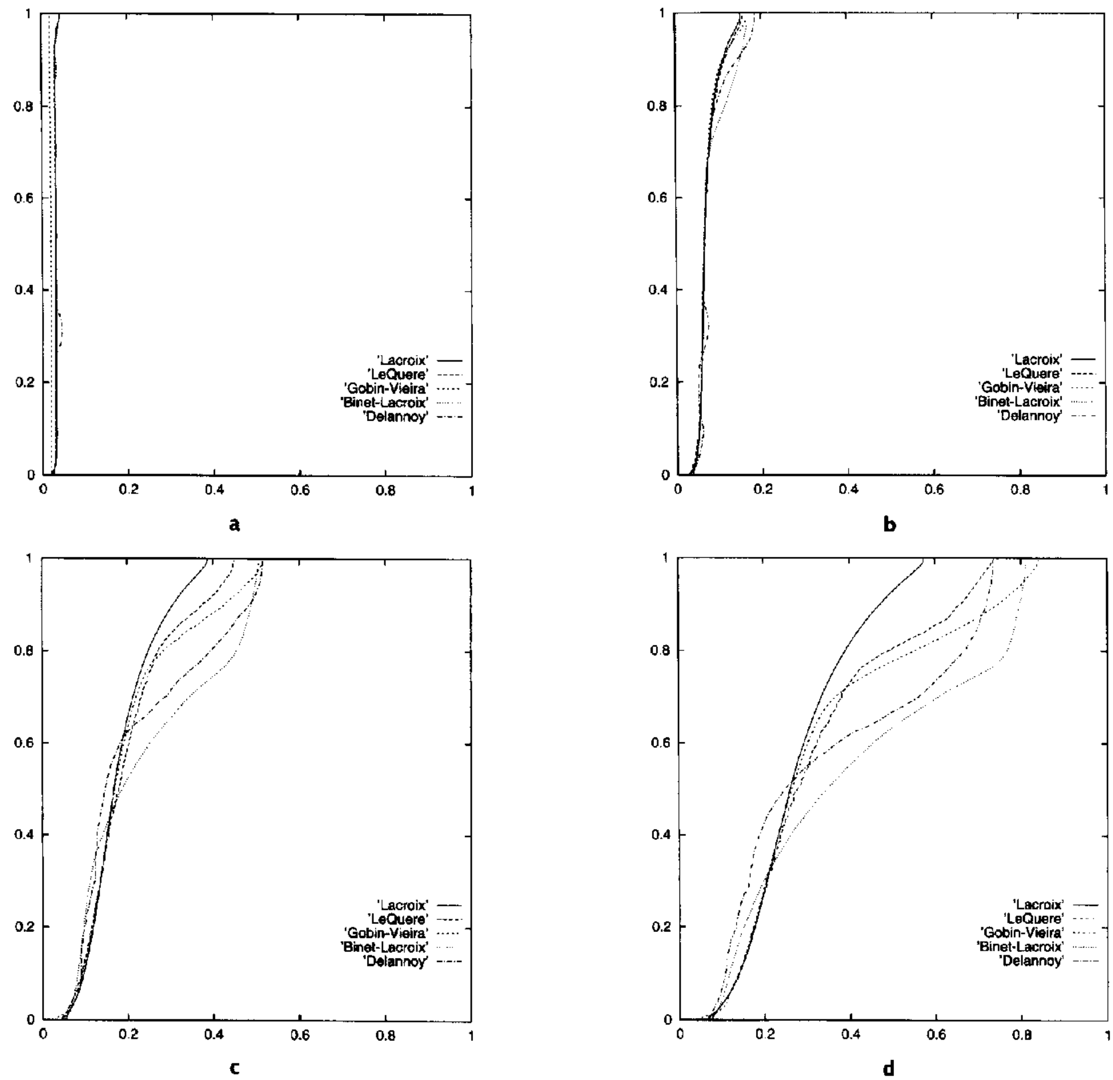

Figure 10. Case 4. Melting front positions. **a)** $Ste\,Fo = 0.0005$. **b)** $Ste\,Fo = 0.002$. **c)** $Ste\,Fo = 0.006$. **d)** $Ste\,Fo = 0.010$.

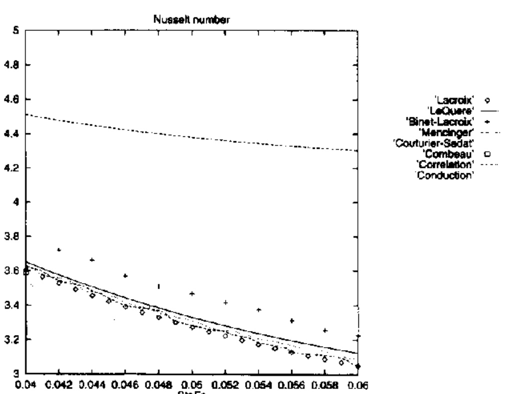

Figure 11. Nusselt number evolution for case 1 (zoom). $Pr = 0.02$. $Ste = 0.01$. $Ra = 2.5{\cdot}10^4$.

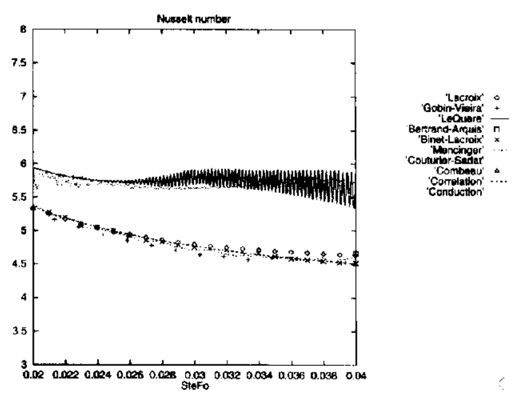

Figure 12. Nusselt number evolution for case 2 (zoom). $Pr = 0.02$. $Ste = 0.01$. $Ra = 2.5{\cdot}10^5$.

cells using a finite-element discretisation. These findings are rather original in the field of convective melting of metals, where most previous numerical studies accept the assumption of quasi-steady flow. Note however that this behaviour has not been reported in the relevant experimental studies.

5.2. The high Prandtl number range (cases # 3 and # 4)

Case # 3 was addressed by six participants, Lacroix, Gobin Viera, Binet-Lacroix, Delannoy, Couturier–Sadat, and Le Quéré and case # 4 by five participants, Lacroix, Gobin–Viera, Binet–Lacroix, Delannoy and Le Quéré. In the high Pr number range, the discrepancies between the numerical results are more important. At $Ra = 10^7$, if one excepts the solution obtained by Delannoy, which has probably to be run on a finer grid, the results for the melted fraction at time t_4 are spread over a ± 18 % range. The differences on the melted fraction are mainly due to the front position in the upper part of the enclosure, since the agreement is still fairly good on the bottom half of the cavity.

At $Ra = 10^8$, again the solution by Delannoy seems to be unsufficiently convergent, and the enthalpy method developed by Binet–Lacroix overestimates the average Nusselt number by more than 30 %. Discarding these solutions, there is still a ± 10 % dispersion on the melted fraction at time t_4 for the three other methods. Examination of the melting front positions at times t_3 and t_4 shows that these three methods are in qualitative agreement for the overall shape of the interface, and that the results agree fairly well in the bottom half of the cavity, while the main differences at the top of the interface are within a ± 20 % range.

6. CONCLUSION

A necessary general remark concerning the present exercise is that the choice of the problem itself (fusion of a pure substance) is such that the front-tracking methods are better adapted to the problem than the fixed grid procedures. The front-tracking methods would however fail to simulate situations where the transition from the liquid to the solid phase is not a macroscopic surface, and enthalpy methods are to be used in most solidification problems where a solid–liquid interfacial region is present between both phases. This problem is not in the scope of the present exercise, which is the simplest that one can think of in this general context and which has been designed to limit the number of parameters to the mainly relevant ones.

As a conclusion to this first stage of the comparison exercise, it may be said that the convergence and accuracy of the methods have to be assessed in more detail. It would of course be of major interest to produce reference solutions for these test cases, and more particularly for case # 4, since case # 2 seems to give rise to unexpected instability and unsteady phenomena for which a reference solution is probably out of reach for some time. By reference solution we mean a solution for which different quantities and in particular the shape of the interface is known at different times with an error bound of, say, ± 5 %. It seems also necessary to investigate in greater detail the effects of the appearance of multiple cells and of unstationary convection on melting of low Prandtl substances, since it can be seen on *figure 12* that the appearance of multiple cell convection not only greatly influences the overall heat transfer, and thus the evolution of the melted fraction, but also the shape of the interface.

A second stage of the exercise is being organized, with a final synthesis within the framework of the Conference on 'Moving Boundaries 99', to be held in Slovenia in June 1999.

Acknowledgements

The authors of this synthesis are grateful to the Ameth network for its support.

REFERENCES

[1] Viskanta R., Heat transfer during melting and solidification of metals, J. Heat Trans.–T. ASME 110 (1988) 1205–1219.

[2] Prescott P., Incropera F.P., Convection heat and mass transfer in alloy solidification, Adv. Heat Trans. 28 (1996) 231–338.

[3] Lacroix M., Voller V.R., Finite difference solutions of solidification phase change problems: transformed vs. fixed grids, Numer. Heat Tr. B-17 (1990) 25–41.

[4] Viswanath R., Jaluria Y., A comparison of different solution methodologies for melting and solidification problems in enclosures, Numer. Heat Tr. B 24 (1993) 77–105.

[5] Voller V.R., An overview of numerical methods for solving phase-change problems, Adv. Numer. Heat Tr. 1 (1987) 341–380.

[6] Gau C., Viskanta R., Melting and solidification of a pure metal from a vertical wall, J. Heat Trans.–T. ASME 108 (1986) 174–181.

[7] Bénard C., Gobin D., Martinez F., Melting in rectangular enclosures: experiments and numerical simulations, J. Heat Trans.–T. ASME 107 (1985) 794–803.

[8] Webb B.W., Viskanta R., Analysis of heat transfer during melting of a pure metal from an isothermal vertical wall, Num. Heat Trans. 9 (1986) 539–558.

[9] Wolff F., Viskanta R., Melting of a pure metal from a vertical wall, Exp. Heat Trans. 1 (1987) 17–30.

[10] Gobin D., Bénard C., Melting of metals driven by natural convection in the melt: influence of the Prandtl and Rayleigh numbers, J. Heat Trans.–T. ASME 114 (1992) 521–524.

[11] Kim C.J., Kaviany M., A numerical method for phase-change problems with convection and diffusion, Int. J. Heat Mass Trans. 35 (1992) 457–467.

[12] Campbell T.A., Koster J.N., Visualization of solid–liquid interface morphologies in gallium subject to natural convection, J. Crystal Growth 140 (1994) 414–425.

[13] Webb B.W., Viskanta R., On the characteristic length sf ale for correlating melting heat transfer data, Int. Comm. Heat Mass Trans. 12 (1985) 637–646.

[14] Beckermann C., Viskanta R., Effect of solid subcooling on natural convection melting of a pure metal, J. Heat Trans.-T. ASME 111 (1989) 416–424.

[15] Jany P., Bejan A., Scaling theory of melting with natural convection in an enclosure, Int. J. Heat Mass Tran. 31 (1988) 1221–1235.

[16] Crank J., Free and moving boundary problems, Clarendon Press, Oxford, 1984.

[17] Lim J.S., Bejan A., The Prandtl number effect on melting dominated by natural convection, J. Heat Trans.-T. ASME 114 (1992) 784–787.

[18] Dantzig J.A., Modelling liquid-solid phase changes with melt convection, Int. J. Numer. Meth. Eng. 28 (1989) 1769–1785.

APPENDIX I

Description of the algorithm used by:

Olivier Bertrand*, Éric Arquis**

MASTER, ENSCPB, BP 108, 33402 Talence cedex, France

Formulation

The unsteady, incompressible, Navier–Stokes equations for both fluid and solid phases are formulated in terms of velocity $\boldsymbol{U}(\mathbf{x},t)$ and pressure $p(\mathbf{x},t)$ as:

– conservation of momentum:

$$\rho\left(\frac{\partial \boldsymbol{U}}{\partial t}+(\boldsymbol{U}\cdot\nabla)\boldsymbol{U}\right) = \rho\, g-\nabla p+\nabla\cdot\big(\mu(\nabla \boldsymbol{U}+\nabla^T \boldsymbol{U})\big)-\beta\,\boldsymbol{U} \quad (1)$$

– conservation of mass:

$$\nabla\cdot\boldsymbol{U}=0 \quad (2)$$

We introduce in the Navier–Stokes equations a source term $S=\beta\,\boldsymbol{U}$ where β takes the value zero if the local solid fraction is zero or 10^{20} if $f_S=1$. For this last case, the source dominates all other terms in the momentum equation and force the velocities to values close to zero.

* bertrand@lmaster.u-bordeaux.fr

** arquis@lmaster.u-bordeaux.fr

The energy equation is formulated in terms of temperature $T(\mathbf{x},t)$ as:

$$\rho\, C_p\left(\frac{\partial T}{\partial t}+\boldsymbol{U}\cdot\nabla\, T\right)=\nabla\cdot(\lambda\nabla T)+\rho\, L\frac{\partial f_S}{\partial t} \quad (3)$$

where f_S is the local solid fraction introduced by Voller in his 'New source scheme'. In this case of an isothermal phase change (at $T=T_f$), the local solid fraction is given by the Heaviside step function:

$$f_S=\begin{cases}0 & \text{if } T>T_f\\ 1 & \text{if } T<T_f\end{cases}$$

Discretisation

Time discretisation

We used a first–order implicit finite-difference scheme for the momentum and energy equations.

Space discretisation

The equations are discretised on a fixed Cartesian mesh by the finite–volume method. The hybrid scheme (first or second–order function of the Péclet number) is used for both diffusive and convective terms. The Navier–Stokes equations are discretised on the usual staggered grid.

Algorithm

The augmented Lagrangian

The discretised Navier–Stokes equations are solved by an augmented Lagrangian method [1] (the Uzawa non-linear algorithm). This is an iterative method between the momentum equations and the pressure field. The Uzawa algorithm consists of an optimisation technique to compute a velocity-pressure saddle point under the incompressibility constraint $\nabla\cdot\boldsymbol{U}=0$.

The 'New source scheme'

The 'New source scheme' [2] is an iterative procedure between the energy equation and the solid fraction update. On the node points where f_S is strictly in the interval]1,0[, we force the solver to return a value for the temperature close to the melting temperature. After that, the solid fraction is updated.

Solution of linear systems

The linear systems are solved by a preconditioned (Jacobi) conjugate gradient method (Bi-CGSTAB) which is an iterative method. Convergence is declared when the residual error is less than 10^{-8} for the momentum equation and 10^{-15} for the energy equation.

Computational parameters

A time step of $\Delta t = 0.01$ s and a 80×80 uniform square grid were used for the case 2. At each time step, the arithmetic mean of the absolute values of $\nabla \cdot \boldsymbol{U}$ at each mesh point is less than 10^{-6}.

REFERENCES

[1] Fortin M., Glowinski R., Méthodes de lagrangien augmenté : applications à la résolution numérique de problèmes aux limites, Dunod, Paris, 1982.

[2] Voller V.R., Fast implicit finite-difference method for the analysis of phase change problems, Numer. Heat Tr. B 17 (1990) 155–169.

APPENDIX II

An enthalpy-porosity technique for the melting problem

Description of the algorithm used by:

Bruno Binet*, Marcel Lacroix**

Département de génie mécanique, université de Sherbrooke, Sherbrooke, J1K 2R1, Québec, Canada

Governing Equations

The mathematical model rests on the following assumptions:

(1) a two-dimensional analysis is applied;

(2) viscous dissipation is neglected;

(3) the flow in the liquid phase is laminar, incompressible and Newtonian;

(4) the Boussinesq approximation for buoyancy is valid;

(5) thermophysical properties are constant and uniform;

(6) volumetric expansion is neglected upon melting;

(7) a no-slip condition holds at all the walls.

With the foregoing assumptions, the governing equations for the conservation of mass, momentum and energy are:

$$\frac{\partial}{\partial x_i}(\rho u_i) = 0 \tag{1}$$

$$\frac{\partial}{\partial t}(\rho u_i) + \frac{\partial}{\partial x_j}(\rho u_j u_i) = \mu \frac{\partial^2 u_i}{\partial x_j \partial x_j} - \frac{\partial p}{\partial x_i} + S_i \tag{2}$$

$$\frac{\partial}{\partial t}(\rho h) + \frac{\partial}{\partial x_j}(\rho u_j h) = \mu \frac{\partial}{\partial x_j}\left(\frac{k}{C}\partial h \, \partial x_j\right) - S_h \tag{3}$$

* bruno.binet@gme.usherb.ca

** marcel.lacroix@gme.usherb.ca

An enthalpy method is retained for the treatment of the melting problem [1–5]. The energy equation for the phase change material (PCM) follows Voller's formulation [1–3] for which the total enthalpy is split into sensible and latent heat components:

$$H(T) = h(T) + L f_l \tag{4}$$

where

$$h(T) = \int_{T_m}^{T} c \, \mathrm{d}T \tag{5}$$

and f_l is the local liquid fraction. Using this formulation, the problems associated with the phase change are isolated in the source term S_h, i.e.:

$$S_h = \rho L \frac{\partial f_l}{\partial t} \tag{6}$$

The liquid fraction f_l is given by the Heaviside step function:

$$\begin{aligned} f_l &= 1 \quad \text{if} \quad h > 0 \\ f_l &= 0 \quad \text{if} \quad h < 0 \end{aligned} \tag{7}$$

The liquid fraction is also used to drive the velocity components to zero in the solid phase of the PCM via the source terms S_x and S_y in the momentum equations (2):

$$\begin{aligned} S_x &= -B(f_l)u \\ S_y &= -B(f_l)v + \rho g \beta (T - T_m) \end{aligned} \tag{8}$$

The function B becomes very large when f_l is zero and goes to zero as f_l tends to one. A function B based on the Carman–Koseny relation for a porous medium as described in references [1–3] is employed:

$$B(f_l) = \frac{C(1 - f_l)^2}{f_l^3 + \varepsilon} \tag{9}$$

with $C = 1.6 \cdot 10^6$ and $\varepsilon = 10^{-3}$. This numerical artifact can be viewed as a way of modelling the transition zone between the solid and liquid phases.

Numerical Procedure

The finite-difference equations are obtained on integrating the conservation equations (1)–(3) over each of the control volumes in the (x,y) plane using second-order centred differences. The convective terms are discretised, however, with a first-order hybrid difference scheme [6] in order to insure stability. The convection coefficients are obtained from the Rhie and Chow interpolation formula [7]. This way, all the equations are solved on a non-staggered grid. The SIMPLEC algorithm [8] is adopted for the velocity–pressure coupling. An implicit Euler scheme is used for the time-stepping procedure. The resulting finite-difference equations for the general dependent variable ϕ at node P have the form:

$$A_P\phi_P - \Sigma_{nb}A_{nb}\phi_{nb} = (SU)_\phi \qquad (10)$$

with: $$A_P = \Sigma_{nb}A_{nb} - (SP)_\phi + \frac{\rho\,\Delta V}{\Delta t} \qquad (11)$$

The set of linearised equations (10) is then solved iteratively with a line by line TDMA solver by sweeping the cavity from left to right. At a given time, convergence is declared when the following three conditions are met: (1) the dimensionless residual for the mass conservation equation is less than $5{\cdot}10^{-3}$; (2) the dimensionless residual for the enthalpy conservation equation is less than than $4{\cdot}10^{-4}$; and (3) the liquid fraction field is stabilised. More stringent convergence criteria were retained but the results, obtained after significantly longer computational times, did not show perceptible changes in the final solution.

The central feature of the present fixed-grid simulation technique for the phase change problem is the source term S_h for the enthalpy equation. This term keeps track of the latent heat evolution and its driving element is the liquid fraction f_l. This fraction takes a value of 1 in fully liquid regions, 0 in fully solid regions and lies in the interval [0,1] in the vicinity of the phase front. In a numerical implementation, its value is determined iteratively from the solution of the enthalpy equation via the following expressions [1–3]:

$$f_{l,P}^{k+1} = f_{l,P}^{k} + \lambda\,\frac{\Delta t\,A_P^k\,h_P^k}{\rho\,L\,\Delta V} \qquad (12)$$

and

$$f_{l,P}^{k+1} = 1 \ \text{ if } \ h_P^k > 0$$
$$f_{l,P}^{k+1} = 0 \ \text{ if } \ h_P^k < 0 \qquad (13)$$

where λ is an under-relaxation factor. The liquid fraction update is applied at every node after the kth solution of the linear system for the enthalpy. At a given time step, the position of the phase front is obtained from the solution of the liquid fraction field by a linear interpolation of the contour line where $f_l = 0.5$.

A constant non-dimensional time step of $2{\cdot}10^{-4}$ and a grid size of 40×40 uniformly distributed nodes were used to carry out the simulation for case # 2. A constant non-dimensional time step of $1.25{\cdot}10^{-5}$ for the first 100 steps (and $2.5{\cdot}10^{-5}$ for the following) and a grid size of 50×181 uniformly distributed nodes in the horizontal and vertical directions respectively were employed to perform the simulations for the melting of paraffin. Computation times on a IBM RS/6000 model 375 ranged from 1 to 9.5 h, depending on the simulated case.

Acknowledgements

The authors are very grateful to the Natural Science and Engineering Research Council (NSERC) of Canada, and the Fonds pour la formation de chercheurs et l'aide à la recherche (FCAR) du Québec for their financial support. The authors also thank the Centre de recherches en calcul appliqué of Montréal (CERCA) and the Centre d'applications du calcul parallèle de l'université de Sherbrooke (CACPUS) for their computer resources.

REFERENCES

[1] Voller V.R., Cross M., Markatos N.C., An enthalpy method for convection/diffusion phase change, Int. J. Numer. Meth. Eng. 24 (1987) 271–284.

[2] Voller V.R., Prakash C., A fixed grid numerical modelling methodology for convection-diffusion mushy region phase-change problems, Int. J. Heat Mass Tran. 30 (1987) 1709–1719.

[3] Brent A.D., Voller V.R., Reid K.J, Enthalpy-porosity technique for modeling convection–diffusion phase change: application to the melting of a pure metal, Numer. Heat Tr. 13 (1988) 297–318.

[4] Binet B., Lacroix M., Numerical simulation of natural convection dominated melting inside uniformly and discretely heated rectangular cavities, Numer. Heat Tr. A 33 (1998) 207–224.

[5] Binet B., Lacroix M., Étude numérique de la fusion dans des enceintes rectangulaires chauffées uniformément ou discrètement par les parois latérales conductrices, Rev. Gén. Therm. 37 (1998) 607–620.

[6] Spalding D.B., A novel finite difference formulation for differential expressions involving both first and second derivatives, Int. J. Numer. Meth. Eng. 4 (1972) 551–559.

[7] Rhie C.M., A numerical study of the flow past an isolated airfoil with separation, Thesis, Dept. of Mechanical and Industrial Engineering, University of Illinois at Urbana-Champaign, 1981.

[8] Van Doormal J.P., Raithby G.D., Enhancements of the SIMPLE method for predicting incompressible fluid flows, Numer. Heat Tr. 7 (1984) 147–163.

APPENDIX III

Description of the algorithm used by:

Hervé Combeau*

LSGMM, École des mines de Nancy, Parc de Saurupt, 54042 Nancy, France

Model

These simulations have been performed with a model developed for the prediction of macrosegregation [1, 2]. This model describes the transport of heat, mass, solute and momentum in the case of the solidification of a binary alloy. For an alloy, the solidification proceeds

* combeau@mines.u-nancy.fr

with a mushy zone. At the macroscopic scale, the thickness of this zone is not negligible and both liquid and solid phases are present inside each macroscopic volume element of the mushy zone. The conservation equations are derived by an averaging technique over a volume element, which is small with regard to the extent of the mushy zone and large with respect to the size of the microstructure of solidification. For the application to the re-melting of a pure substance, the transport of solute has been neglected. Assuming that the solid phase is fixed, the density of the liquid phase is constant except in the buoyancy term, the density of the solid phase is equal to the density of the liquid, the specific heat of the solid and liquid phases are constant and equal, the viscosity is constant, then the complete set of equation is:

heat conservation equation:

$$\rho_{\text{ref}} \frac{\partial h}{\partial t} + \rho_{\text{ref}} C_P \vec{V} \nabla T = \text{div}(\lambda \nabla T) \tag{1}$$

– mass conservation equation:

$$\text{div}(\vec{V}) = 0 \tag{2}$$

– momentum conservation equation for the liquid phase:

$$\begin{aligned} &\rho_{\text{ref}} \frac{\partial \vec{V}}{\partial t} + \frac{\rho_{\text{ref}}}{g_{\text{L}}} (\vec{V} \nabla) \vec{V} \\ &= \mu \Delta \vec{V} - g_{\text{L}} \nabla p - g_{\text{L}} \frac{\mu}{K} \vec{V} - \rho_{\text{ref}}\, \beta\, (T - T_{\text{ref}})\, g_{\text{L}}\, \vec{g} \end{aligned} \tag{3}$$

$\vec{V}$ is the superficial velocity of the liquid phase, T the temperature, and h the averaged mass enthalpy defined as:

$$h = C_P T + g_{\text{L}} L_{\text{F}} \tag{4}$$

where C_P is the mass specific heat, g_{L} the volume fraction of liquid and L_{F} the latent heat of melting of the pure substance. In equation (3), K is the permeability of the mushy zone, it accounts principally for the drag force of the solid skeleton on the interdendritic liquid. The permeability is approximated by the Carman–Kozeny relationship:

$$K = \frac{\lambda - 2^2 g_{\text{L}}^3}{180\,(1 - g_{\text{L}})^2} \tag{5}$$

λ_2 is the secondary dendrite arm spacing. As can be seen, the permeability tends toward infinity when the liquid volume fraction becomes unity, thus reducing equation (3) to the standard Navier–Stokes equation. At an increasing volume fraction of solid, the permeability tends toward zero and the drag force of the solid skeleton dominates the other contributions appearing in equation (3).

In order to close the set of equations, a supplementary relation between T and g_{L} is needed. As this model deals with an alloy, a solidification range has to be defined. In the case of a pure substance, this solidification range is artificial. The relation which has been used is the following:

$$\begin{aligned} &\text{if } \ T < T_{\text{F}}, \ g_{\text{L}} = 0 \\ &\text{if } \ T_{\text{F}} \leqslant T \leqslant T_{\text{F}} + \varepsilon, \ g_{\text{L}} = \frac{T - T_{\text{F}}}{\varepsilon} \\ &\text{if } \ T > T_{\text{F}}, \ g_{\text{L}} = 1 \end{aligned} \tag{6}$$

where T_{F} is the temperature of melting of the pure substance.

Discretisation method

A control volume method has been used for the discretisation of the conservation equations [1–3]. The total flux (convection plus diffusion) on the faces of the control volume have been estimated using a power law scheme [3]. The SIMPLEC algorithm has been adopted to treat the velocity pressure coupling. A specific algorithm is needed to deal with the non-linearity of the heat conservation equation. Equation (1) is integrated in its natural form, i.e., with two main variables: the mass average enthalpy and the temperature. Using the nomenclature of the finite–volume formulation of Patankar [3], the integration of equation (1) in time and space over a control volume can be written as:

$$\begin{aligned} &a_{\text{P}}^0 h_{\text{P}}^{t+\Delta t} + (a_{\text{E}} + a_{\text{W}} + a_{\text{N}} + a_{\text{S}}) T_{\text{P}}^{t+\Delta t} \\ &= a_{\text{E}} T_{\text{E}}^{t+\Delta t} + a_{\text{W}} T_{\text{W}}^{t+\Delta t} + a_{\text{N}} T_{\text{N}}^{t+\Delta t} + a_{\text{S}} T_{\text{S}}^{t+\Delta t} + a_{\text{P}} h_{\text{P}}^{t} \end{aligned} \tag{7}$$

The average enthalpy has been chosen as the principal variable in equation (6) [1]. Since all transfers are coupled, an iterative procedure is used as follows: (1) compute h from equation (1); (2) compute V from equation (3); (3) compute p from equation (2) and correct the velocity field in order to verify the global mass conservation; (4) compute T and g_{L} from equation (6). This sequence of operations is repeated until convergence is achieved before advancing to the next time–step.

Calculation parameters

Time–step until 500 s: 0.01 s
Time step after 500 s: 0.1 s
$\lambda_2 = 10^{-6}$ m
Solidification range: $\varepsilon = 0.1$ °C
Number of nodes in X direction: 50
Number of nodes in Y direction: 50.

The location of the melting front has been defined as the location of the volume fraction of liquid: 0.99.

REFERENCES

[1] Ahmad N., Combeau H., Desbiolles J.-L., Jabanti T., Lesoult G., Rappaz J., Rappaz M., Stomp C., Numerical

simulation of macrosegregation: a comparison between FVM and FEM predictions and a confrontation with experiments, Metal. Mater. Trans. A 29 (1998) 617–630.

[2] Vannier I., Combeau H., Lesoult G., Numerical model for prediction of final composition of heavy steel ingots, Mat. Sci. Eng. A-Struct. 173 (1993) 317.

[3] Patankar S.V., Numerical Heat Transfer and Fluid Flow, Hemisphere, Washington DC, 1980.

APPENDIX IV
Description of the algorithm used by:

Yves Delannoy*

EPM/Madylam

BP 95, 38402 Saint-Martin-d'Hères cedex, France

The simulations are performed using FLUENT UNS 4.2 and user-defined routines. The main features of the method are:

– one-domain approach;

– enthalpy formulation; true unstationary procedure, based on the source term method by Voller (in the momentum equation, this term is a friction term, similar to a porosity);

– implicit time discretisation (order 1, iterative convergence at each time-step), second-order space discretisation, uncentered convective terms;

– definition of the interface as the 0.5 solid fraction;

– no coordinate transformation; phase change interval is 1 % of the overall ΔT;

– autoadaptive triangular grid and non-conform grid refinement at the interface and unrefinement behind the front (initially 3 300 triangles);

– initialization at $T_F - 0.001\Delta T$; resolution by the SIMPLEC algorithm;

– algebraic matrix multigrid solver;

– run on workstation SUN UltraSparc 170 (9 Specfp95), in about 2 CPU hours.

APPENDIX V
A front-tracking method for convective melting of pure substances

Description of the algorithm used by:

Dominique Gobin** and Gisele Vieira***

FAST

Bât. 502, campus universitaire, 91405, Orsay cedex, France

* delannoy@hmg.inpg.fr

** gobin@fast.u-psud.fr

*** gvieira@iis.com.br

Problem definition and hypotheses

The coupled problem to be solved is described by the set of equations governing natural convection in the non-rectangular liquid domain (Navier–Stokes, energy and continuity equations), and by the local energy balance equation at the interface.

The solution procedure uses a front immobilisation technique based on the widespread quasi-steady and quasi-stationary hypotheses, which allow:

(1) to solve separately the fluid flow and the interface motion,

(2) to solve the steady state equations of natural convection in the melt.

These assumptions have been shown to be relevant in applications concerning high Prandtl number liquids and relatively high Rayleigh numbers (Ra based on H above 10^6) [1]. For high Prandtl numbers, the thermal boundary layers separate very early in the melting process and arguments based on scaling considerations show that the melting front velocity is several orders of magnitude smaller than the velocities in the boundary layers [2], justifying the first hypothesis. As for the second assumption, studies on transient natural convection of a fluid in a fixed enclosure [3] show that the orders of magnitude of the time scales for natural convection to reach steady state are much smaller than the time scales of the melting process.

In the case of liquid metals, the use of the dimensionless group $Ra \times Pr$ proposed by Bejan [3] can be applied to the separate boundary layer regime. On the other hand, for this range of Prandtl numbers, the time scales for transient natural convection in enclosures are not well-known and complex behaviour may be expected.

Under the assumptions mentioned above, the complete set of equations to be solved is then:

– in the liquid cavity:

$$\nabla \cdot \underline{\boldsymbol{V}} = 0 \qquad (1)$$

$$(\underline{\boldsymbol{V}} \cdot \nabla)\underline{\boldsymbol{V}} = \nabla^2 \underline{\boldsymbol{V}} - \nabla P + Gr_H\, \theta\, \underline{\boldsymbol{k}} \qquad (2)$$

$$(\underline{\boldsymbol{V}} \cdot \nabla)\, \theta = \frac{1}{Pr} \nabla^2 \theta \qquad (3)$$

– at the interface, the energy balance equation:

$$\nabla\theta \cdot \underline{\boldsymbol{n}} = \rho^* \frac{\partial c}{\partial \tau} \qquad (4)$$

where $\partial c/\partial \tau\, (\tau = Fo\, Ste)$ is the local velocity of the melting front along $\underline{\boldsymbol{n}}$, the normal vector to the interface. Dirichlet thermal boundary conditions are taken on the vertical wall and at the interface, and the horizontal walls are adiabatic. In the liquid cavity, zero velocity dynamic boundary conditions are considered at the four walls.

Equations (1–4) have been set in a dimensionless form using the height H of the enclosure as the reference length and the kinematic viscosity ν in velocity scales.

Numerical procedure

Flow field calculation

The system of non-linear equations (1–3) governing natural convection in the irregular liquid cavity is transformed using a classical algebraic non-orthogonal transformation of co-ordinates (see Sparrow et al. [4]). The transformed equations are discretised on a square computational domain, using the hybrid differencing scheme [5]. The SIMPLE algorithm is used to solve the pressure-velocity coupling and the solution of the discretised equations is obtained with an ADI procedure.

The co-ordinate transformation introduces the successive derivatives of the function $C(z)$ up to the third order and cross-terms in the calculation of the heat fluxes at the surface of the control volumes. All these terms are retained and the discretised conservation equation for a given control volume leads to a 9-point formulation. In order to take advantage of the ADI procedure, a 5-point implicit formulation has been kept and the 4 non-adjacent points arising from the cross-terms are shifted to the right-hand side of the equations. A detailed description of the discretisation technique may be found elsewhere [6].

The grid defined on the square computational domain may be irregularly spaced, in order to provide better resolution of the velocity and temperature gradients at the solid walls. The 60×42 grid used in our computations has a sinusoidal distribution in the horizontal x-direction and a regularly spaced distribution in the vertical z-direction.

Interface motion

When the temperature and flow fields converge in the liquid domain, the local heat transfer at the interface is calculated at the grid points and interpolated at 100 equally-spaced z-positions using a cubic spline. As the cold wall is considered to be at the fusion temperature, and the solid phase is isothermal, the melting front movement is explicitly calculated from the local heat transfer at the interface, which is assumed to be constant during the calculation of the new melting front position. Smaller time–steps are considered at the beginning of the process to make sure that the quasi-stationary hypothesis does not artificially increase the melting front velocity. The new liquid cavity is defined at the 100 equally-spaced nodes: the interface position $C(z)$ at the grid points and the nodal values of the successive derivatives of $C(z)$ required for the calculation of the transformation coefficients are obtained from cubic spline interpolation.

Initialisation

The initialisation of the process uses the classical Neumann solution of the 1D Stefan problem where pure conduction is considered to be the only heat transfer mode. This solution is relevant as far as natural convection has not developed in the melt, and the heat transfer distribution at the interface is uniform. For a given height of the enclosure and a given Rayleigh number, this solution may be used up to a maximum width δ of the liquid cavity. In the absence of a criterion to determine this value, we performed a number of numerical calculations in rectangular enclosures, for a given Ra_H and different aspect ratios. We found that the heat transfer was still very close to the pure conduction solution in a cavity of aspect ratio $H/\delta = 8$ for $Ra_H \approx 10^5$, and $H/\delta = 12.5$ for $\mathrm{Ra}_H \approx 10^6$. The calculation is then initialised with a rectangular cavity of width δ and the corresponding time is given by the Neumann solution.

The numerical results presented below have been obtained on a HP-735 computer. Typical values of the fusion time step $\delta\tau_F$ increase from about 10^{-3} at the beginning of the process to about 10^{-2} in the convection regime.

REFERENCES

[1] Gadgil A., Gobin D., Analysis of two dimensional melting in rectangular enclosures in presence of convection, J. Heat Trans.-T. ASME 106 (1984) 20–26.

[2] Bénard C., Gobin D., Martinez F., Melting in rectangular enclosures: experiments and numerical simulations, J. Heat Trans.-T. ASME 107 (1985) 794–803.

[3] Bejan A., Convection Heat Transfer, 2nd Edition, Wiley Science, New York, 1995.

[4] Sparrow E.M., Patankar S.V., Ramadhyani S., Analysis of melting in the presence of natural convection in the melt region, J. Heat Trans.-T. ASME 99 (1977) 520–526.

[5] Patankar S.V., Numerical Heat Transfer and Fluid Flow, Hemisphere, Washington DC, 1980.

[6] Manseur A., Étude numérique de la convection naturelle dans des domaines irréguliers confinés, Thèse, Université Paris-VI, 1988.

APPENDIX VI

An Eulerian–Lagrangian method for the melting problem

Description of the algorithm used by:

Marcel Lacroix*

Département de génie mécanique, université de Sherbrooke, Sherbrooke, Québec, Canada, J1K 2R1

* marcel.lacroix@gme.usherb.ca

Problem Statement

The dimensionless conservation equations for mass, momentum, and energy are formulated in terms of the stream function ψ, vorticity ω and temperature θ. The resulting transport equations for the flow property ϕ take the following form in Cartesian co-ordinates:

$$\frac{\partial(\rho\phi)}{\partial t} + \frac{\partial}{\partial x}\left(u\phi - \Gamma\frac{\partial\phi}{\partial x}\right) + \frac{\partial}{\partial y}\left(v\phi - \Gamma\frac{\partial\phi}{\partial y}\right) = S(x,y) \quad (1)$$

$S(x,y)$ is a source term, Γ is an exchange coefficient, and ρ is a constant. The variable ϕ and its corresponding parameters are given explicitly in *table I*. The velocity components u and v in the liquid phase of the PCM are given by:

$$u = \frac{\partial\psi}{\partial y}\ ,\ v = -\frac{\partial\psi}{\partial x} \quad (2)$$

The vorticity is defined as usual as:

$$\omega = \frac{\partial v}{\partial x} - \frac{\partial u}{\partial y} \quad (3)$$

In addition, an energy balance for the solid-liquid PCM interface yields the following dimensionless condition for the moving boundary:

$$-\nabla\theta\cdot\vec{n} = \frac{\rho^*}{Ste}v_n \quad (4)$$

where v_n is the dimensionless local normal interface velocity and $\nabla\theta\cdot\vec{n}$ is the local normal heat flux to the solid liquid interface.

Numerical Procedure

As melting progresses, the moving solid liquid interface becomes distorted. As a result, its curvilinear shape will not, in general, coincide with the grid nodes on a rectangular Cartesian mesh. To overcome this problem, the general conservation equation equation (1) and its boundary conditions are transformed from the original Cartesian grid (x,y) to a curvilinear grid (ξ,η). The resulting conservation equations are slightly more complicated, but their boundary conditions are specified on straight boundaries, and the computational grid is rectangular and uniformly spaced. Adopting this technique [1–3], equation (1) becomes in the transformed co-ordinate system:

$$\begin{aligned}
&\frac{\partial(\rho\phi)}{\partial t} + \frac{1}{J}\frac{\partial\rho\phi}{\partial\xi}\left[\frac{\partial x}{\partial\eta}\frac{\partial y}{\partial t} - \frac{\partial y}{\partial\eta}\frac{\partial x}{\partial t}\right] \\
&-\frac{1}{J}\frac{\partial\rho\phi}{\partial\eta}\left[\frac{\partial y}{\partial\xi}\frac{\partial x}{\partial t} - \frac{\partial x}{\partial\xi}\frac{\partial y}{\partial t}\right] \\
&+\frac{1}{J}\frac{\partial}{\partial\xi}\left[(U\phi) - \frac{\Gamma}{J}\left(\alpha\frac{\partial\phi}{\partial\xi} - \beta\frac{\partial\phi}{\partial\eta}\right)\right] \\
&+\frac{1}{J}\frac{\partial}{\partial\eta}\left[(V\phi) - \frac{\Gamma}{J}\left(\gamma\frac{\partial\phi}{\partial\eta} - \beta\frac{\partial\phi}{\partial\xi}\right)\right] = S(\xi,\eta) \quad (5)
\end{aligned}$$

The geometric factors U, V, α, β, γ and the Jacobian J of the transformation are defined as follows :

$$U = \frac{\partial\psi}{\partial\eta},\ V = -\frac{\partial\psi}{\partial\xi},\ J = \frac{\partial x}{\partial\xi}\frac{\partial y}{\partial\eta} - \frac{\partial x}{\partial\eta}\frac{\partial y}{\partial\xi}$$

$$\alpha = \left(\frac{\partial x}{\partial\eta}\right)^2 + \left(\frac{\partial y}{\partial\eta}\right)^2,\ \beta = \frac{\partial x}{\partial\xi}\frac{\partial x}{\partial\eta} - \frac{\partial y}{\partial\eta}\frac{\partial y}{\partial\xi}$$

$$\gamma = \left(\frac{\partial x}{\partial\xi}\right)^2 + \left(\frac{\partial y}{\partial\xi}\right)^2$$

The source term $S(\xi,\eta)$ for the vorticity equation (*table I*) becomes:

$$S(\xi,\eta) = \frac{Ra\,Pr}{J}\left[\frac{\partial y}{\partial\eta}\frac{\partial\theta}{\partial\xi} - \frac{\partial y}{\partial\xi}\frac{\partial\theta}{\partial\eta}\right] \quad (6)$$

The Stefan condition, equation (4), is now rewritten as:

$$-\frac{1}{J}\frac{\partial y}{\partial\eta}\frac{\partial\theta}{\partial\xi} = \frac{\rho^*}{Ste}\frac{\mathrm{d}s(y,t)}{\mathrm{d}t} \quad (7)$$

where $s(t,y)$ represents the time-dependent position of the solid–liquid interface. The finite difference equations are obtained on integrating the general governing equation, equation (5), over each of the control volumes in the (ξ,η) plane. The resulting finite–difference scheme has the form:

$$\begin{aligned}
&ASW\phi_{SW} + AS\phi_S + ASE\phi_{SE} + AP\phi_P \\
&+AE\phi_E + ANW\phi_{NW} + AN\phi_N + ANE\phi_{NE} - Q = 0 \quad (8)
\end{aligned}$$

Expressions for the coefficients in equation (8) may be found in [3]. The terms arising from the non-orthogonality of the grid appear in the coefficients of the crossed terms ASW, ASE, ANW, and ANE. Q contains the source term S and the value ϕ_P from the previous time-step. The advection-diffusion part of coefficients AS, AW, AP, AE and AN is modified for stability according to the power law scheme of Patankar [4]. The linearised equations are solved iteratively for θ, ω and ψ using a line-by-line tridiagonal matrix algorithm. Convergence is declared, at a given time step, when the largest residual for all difference equations, i.e., the left hand side of equation (8), is smaller than ε (ε is a small number of the order of 10^{-3}). Its magnitude depends on the equation and the problem to be solved (Rayleigh number, grid size and time–step). For the cases presented here, ε was chosen so that the solutions obtained with more stringent convergence criteria did not reveal perceptible changes.

The numerical solution proceeds through a series of small time intervals during which the solid liquid interface is assumed to be fixed. For each such time interval, the field equations are solved implicitly (retaining the unsteady terms in equation (5) in the now-fixed computational domain. The solution of the field equations provides the energy fluxes at the interface after that time interval. The horizontal displacement of the interface can then be calculated explicitly from equation (7), and a new computational grid is generated for the next time step. The grid is generated algebraically using a power law clustering function that concentrates grid nodes in the vicinity of the wall-PCM interface and in the vicinity of the phase front [1].

A constant non-dimensional time step of $2{\cdot}10^{-4}$ and a grid size of 21×25 non-uniformly distributed nodes in the horizontal and vertical directions respectively were used to carry out the simulations for the melting of the metal. A constant non-dimensional time-step of $2{\cdot}10^{-5}$ and a grid size of 25×35 non-uniformly distributed nodes were employed to perform the simulations for the melting of n-octadecane.

Acknowledgements

The author is grateful to the Natural Science and Engineering Research Council of Canada for its support of this research.

REFERENCES

[1] Lacroix M., Garon A., Numerical solution of phase change problems: an Eulerian–Lagrangian approach, Num. Heat Trans. B 19 (1992) 57–78.

[2] Lacroix M., Arsenault A., Analysis of natural convection melting of a subcooled pure metal, Num. Heat Trans. A 23 (1994) 21–34.

[3] Lacroix M., Coupling of wall conduction with natural convection-dominated melting of a phase change material, Num. Heat Trans. A 26 (1994) 483–498.

[4] Patankar S.V., Numerical Heat Transfer and Fluid Flow, Hemisphere, Washington DC, 1980.

APPENDIX VII

Description of the algorithm used by:

Patrick Le Quéré*

Limsi, BP 133, 91403 Orsay cedex, France

Formulation of the equations

The Navier–Stokes equations are written in velocity–pressure formulation, and the enthalpy form of the energy equation is used. These equations are written on a domain Ω which expands in time in the horizontal direction, i.e., $\Omega = [0, X_{\mathrm{R}}(t)] \times [0,1]$. The position of the right boundary $X_{\mathrm{R}}(t)$ is assumed to vary linearly in time $X_{\mathrm{R}}(t) = X_{\mathrm{R}}(0) + \mathbf{w}t$. The equations in dimensionless form read:

$$\frac{\partial \mathbf{v}}{\partial t} + \mathbf{v}\nabla\cdot\mathbf{w} + \nabla(\mathbf{v}-\mathbf{w})\mathbf{v} = -\nabla P + \frac{Pr}{Ra^{1/2}}\nabla^2\mathbf{v} + Pr\,\mathbf{k}\Theta \text{ in } \Omega \quad (1)$$

$$\nabla\cdot\mathbf{v} = 0 \text{ in } \Omega \quad (2)$$

$$\frac{\partial h}{\partial t} + h\nabla\cdot\mathbf{w} + \nabla(\mathbf{v}-\mathbf{w})\,h = \frac{1}{Ra^{1/2}}\nabla\cdot\lambda\nabla\theta \text{ in } \Omega \quad (3)$$

where $\mathbf{v}$ is the absolute velocity in the moving frame, h the enthalpy and Θ the temperature. The reference quantities are H for lengths and $\frac{\kappa_{\mathrm{f}}}{H}Ra^{1/2}$ for velocity and related scales for time and pressure where κ_{f} is the fluid thermal diffusivity $\left(= \frac{\lambda_{\mathrm{f}}}{(\rho C_p)_{\mathrm{f}}}\right)$. The dimensionless temperature Θ is defined as $\frac{T - T_{\mathrm{f}}}{T_h - T_{\mathrm{f}}}$ and the reference enthalpy difference is $(\rho C_p)_{\mathrm{f}}\,(T_{\mathrm{h}} - T_{\mathrm{f}})$. h is the dimensionless enthalpy, which is a discontinuous function of the temperature. It is approximated by the following function $\tilde{h}$:

$$\tilde{h} = \left(\frac{1}{St\,\Theta_{\mathrm{r}}} + 1\right)\Theta \quad \text{for} \quad 0 \le \Theta \le \Theta_{\mathrm{r}} \quad (4)$$

$$\tilde{h} = \frac{1}{St} + \Theta \quad \text{for} \quad \Theta_{\mathrm{r}} \le \Theta \le 1 \quad (5)$$

where Θ_{r} is a prescribed (small) regularisation temperature. $\tilde{h}$ is continuous and piecewise linear.

Discretisation

Time discretisation

The time discretisation combines an implicit treatment of the viscous or diffusive terms with an explicit discretisation for the convective terms. The source term corresponding to the expanding mesh is treated implicitely. Applied to a scalar equation of the form:

$$\frac{\partial f}{\partial t} + f\nabla\cdot\mathbf{w} + \nabla(\mathbf{v}-\mathbf{w})f = \frac{1}{Ra^{1/2}}\nabla^2 f \quad (6)$$

the fully time discretised formulation is:

$$\frac{3f^{n+1} - 4f^n + f^{n-1}}{2\Delta t} + f^{n+1}\nabla\cdot\mathbf{w} + 2\nabla(\mathbf{v}-\mathbf{w})f^{n+1} - \nabla(\mathbf{v}-\mathbf{w})f^n = \frac{1}{Ra^{1/2}}\nabla^2 f^{n+1} \quad (7)$$

where n stands for the time index. This results in a Helmholtz equation for f^{n+1}:

$$\left(\frac{1}{Ra^{1/2}}\nabla^2 - \frac{3}{2\Delta t} - \nabla\cdot\mathbf{w}\right) f^{n+1} = S_{\mathrm{f}}^{n,n-1} \quad (8)$$

* plq@limsi.fr

Space discretisation

The equations are discretised on a uniform mesh in both directions using the usual staggered grid arrangement. Second–order centred discretisations are used for the diffusive and convective terms.

Solution of linear systems

The resulting linear system is solved using either an ADI or a GMRES type solver.

It is convenient to define a phase indicator which is set to 1 when $\Theta > \Theta_r$ and to 0 otherwise. Cells characterised by phase values of 1 and 0 are liquid and solid respectively.

For both velocity components, the above procedure readily applies except that the linear system is modified so that the velocities resulting from the inversion are zero in the solid or at the boundaries between solid and fluid cells.

The enthalpy equation is solved over all Ω. In this case the dummy variable f in (6) stands for $(\rho C_p)_f(\Theta)\,\Theta$. The discrete equations resulting from the time and space discretisations form a nonlinear system for the temperatures Θ_{ij}^{n+1}, due to the fact that the equivalent thermal capacity, defined as $\frac{\bar{h}}{\Theta}$ (cf. equations (4) and (5)), depends on the temperature. This nonlinear system is solved iteratively (i.e., its coefficients are updated at each iteration) using overrelaxation until a prescribed accuracy is met.

Incompressibility constraint

The incompressibility constraint is maintained through a prediction–projection algorithm. In the prediction step, both velocity components are solved independently, using P^n in the source term. The resulting velocity field $\boldsymbol{V}^*$ is then projected onto the subspace of divergence free vector fields using the Helmholtz decomposition:

$$\boldsymbol{V}^{n+1} - \boldsymbol{V}^* = \Delta t\,\nabla\phi \qquad (9)$$

which can be done by computing:

$$\nabla^2\phi = -\frac{\nabla\cdot\boldsymbol{V}^*}{\Delta t} \qquad (10)$$

with homogeneous Neuman boundary conditions. The phase indicator can be used to impose this condition exactly at the fluid solid interface. This elliptic equation is solved using a multigrid algorithm, in which the phase indicators and linear operators on the coarser grids are defined recursively from those on the finer grid.

Algorithm

- beginning of time–step
- compute new grid positions and geometrical quantities
- solve for the new temperature field Θ^{n+1}
- update phase indicator
- compute the intermediate velocities $\boldsymbol{V}^*$ using Θ^{n+1} in the buoyancy force
- compute its divergence $\nabla\cdot\boldsymbol{V}^*$
- solve for the pressure correction ϕ
- update velocities and pressure (c.f 9):

$$\boldsymbol{V}^{n+1} = \boldsymbol{V}^* + \Delta t\,\nabla\phi$$
$$P^{n+1} = P^n + \frac{3}{2}\phi$$

- extrapolate new temperature and thermal capacity end of time–step.

Determination of the front position

As said above, all cells whose temperature is larger than Θ_r are considered as liquid, and the surface of these cells is defined as the melt fraction. The position of the interface is defined at the location between a liquid and a solid cell. Θ_r was generally chosen as 0.001.

Computational parameters

Most of the computations were performed with $\Delta t = 0.01$ in units of $\frac{H^2}{\kappa_f}Ra_H^{-1/2}$. The computations for the paraffin were done using a spatial resolution 128×128 or 192×192, those for the metal with 128×192. For the paraffin the right boundary was prescribed to move from 0.1 to 0.8 over the timelength t_4, and from 0.2 to 0.6 for the metal.

APPENDIX VIII

Description of the algorithm used by:

Marc Médale*

Iusti, UMR CNRS 6595, Technopole de Château-Gombert, 13453 Marseille cedex 13, France

The method uses a finite-element technique with a one-domain approach and an Eulerian description (fixed grid, eventually complex and unstructured).

The energy equation is written in the enthalpy form and the latent heat contribution appears as a source term (Voller and Prakash). This model is particularly well suited to non-isothermal phase change processes. The temperature–enthalpy relation is piecewise linear. The flow model uses a primitive variables formulation with a quadratic approximation for the velocity and a linear approximation for pressure (discontinuous by elements).

medale@iusti.univ-mrs.fr

Space discretisation is the same for the two cases considered in this preliminary approach 40×40 elements, that is 81×81 calculation nodes, while the dimensionless time step 0.001 for case # 1 and 0.0001 for case # 2.

The determination of the front position is made through the solid fraction, which depends linearly on temperature. The phase change interval is 0.001, in order to simulate the isothermal melting process.

The linear system of equations is solved using an unstationary decoupled approach, which consists of sequentially solving, at each time-step, the energy equation using the latest available velocity field, and then the flow problem using the latest temperature field. We thus can use different techniques to solve the energy equation and the Navier–Stokes equations. For a sequential execution of the code on a monoprocessor, the direct resolution of the linear algebraic systems is faster. The parallel execution on a multiprocessor uses a different solution method for each system:

– energy equation: a BCGS iterative method BCGS (bi-conjugate gradient squared) preconditionned by an ASM (additive Schwartz method).

– incompressible Navier–Stokes equations: iterative BCGS method, preconditionned by the SSOR (symmetric successive over-relaxation) method.

APPENDIX IX

Description of the algorithm used by:

Jure Mencinger*, Božidar Šarler

LFDT

University of Ljubljana, Aškerčeva 6, 1000 Ljubljana, Slovenia

Formulation of the equations

The continuum model [1] is used for the calculation of the unknown fields. It is assumed that the liquid fraction f_l varies with the temperature Θ as:

$$f_l = \begin{cases} 0, & \Theta \leqslant 0 \\ \Theta/\Delta_\Theta, & \Delta_\Theta > \Theta > 0 \\ 1, & \Theta \geqslant \Delta_\Theta \end{cases} . \tag{1}$$

Δ_Θ is the prescribed melting interval (set to 10^{-3}). The velocity field is determined through the mixture momentum conservation equation with solid phase velocity set to zero ($\boldsymbol{v}_s = 0$):

$$\frac{\partial \mathbf{v}}{\partial Fo} + \nabla\cdot(\mathbf{v}\mathbf{v}) = -\nabla p + Pr\nabla^2\mathbf{v} + Pr\,Ra\,f_l\,\Theta\,\boldsymbol{j} \\ -\nabla\cdot(\mathbf{v}(\mathbf{v}_l - \mathbf{v})) - \gamma(1 - f_l)\mathbf{v} \tag{2}$$

where $\boldsymbol{v}$ and p stand for non-dimensional mixture velocity and pressure, respectively. The last term insures zero velocity of solid phase (γ is set to 10^9 in the calculation).

The mixture energy conservation equation is written in the enthalpy form:

$$\frac{\partial h}{\partial Fo} + \nabla\cdot(\mathbf{v}h) = \nabla^2 h - \frac{1}{Ste}\nabla^2 f_l - \frac{1}{Ste}\nabla\cdot(\mathbf{v}(h_l - h)) \tag{3}$$

The temperature field is calculated from the enthalpy field by inverting the relation:

$$h = \Theta + \frac{f_l}{Ste} \tag{4}$$

Discretisation

Space discretisation

The equations are discretised using standard control volume (CV) method as proposed by Patankar [2]. The grid used for this calculation was non-uniform with CV faces located midway between the grid points. For the calculation 100×80 internal grid points were used. Grid spacing is described by the relations:

$$\mathrm{d}x_{i+1} = \alpha_x\,\mathrm{d}x_i \qquad \text{and} \qquad \mathrm{d}y_{j+1} = \alpha_x\,\mathrm{d}y_j \tag{5}$$

with $\mathrm{d}x_i$ and $\mathrm{d}y_j$ representing the dimensions of the (i,j)-th control volume. The parameter α takes values: $\alpha_x = 1.0414$ for $0.0 \leqslant x \leqslant 0.3$, $\alpha_x = 1.00$ for $0.3 < x \leqslant 1.0$, $\alpha_y = 1.02$ for $0.0 \leqslant x \leqslant 0.5$ and $\alpha_y = 0.98$ for $0.5 < x \leqslant 1.0$. A standard staggered grid was used for the calculation of the velocity field. An upwind scheme was used for the convection terms.

Time discretisation

The simple first-order Euler implicit scheme is used for obtaining the values at each time-step. The resulting system of algebraic equation is solved iteratively with the alternating direction tridiagonal matrix algorithm (TDMA).

Algorithm

Algorithm can briefly be described by the following steps:

(1) initialisation: $t = 0$, $\mathbf{v} = 0$, $h = 0$, $\Theta = 0$, $f_l = 0$

(2) beginning of the time-step: $t = t + \Delta t$

(3) solve the equation for the velocity field (with SIMPLER)

(4) solve the equation for the enthalpy field

(5) calculate temperature field Θ

(6) calculate liquid fraction field f_l

* jure.mencinger@fs.uni-lj.si

(7) *if* the solution for the time–step has converged *goto* step 2 *else goto* step 3.

The convergence at the time–step is determined by the criterion:

$$\frac{\max\limits_{i,j}\left(\phi_{i,j}^{n+1}-\tilde{\phi}_{i,j}^{n+1}\right)}{\left|\max\limits_{i,j}\left(\phi_{i,j}^{n+1}\right)-\min\limits_{i,j}\left(\phi_{i,j}^{n+1}\right)\right|}\leq\varepsilon_{\text{timestep}} \qquad (6)$$

where ϕ^{n-1} is the matrix representing the values of the newly calculated field (u, v or h) and $\tilde{\phi}^{n+1}$ the field from the previous iteration. The value of $\varepsilon_{\text{timestep}}$ was set to 10^{-4}. The time–step size used was 10^{-6} ($t = Ste\,Fo$). All further details are elaborated in [3].

Determination of the front position

The position of the solid-liquid interface is assumed to be the curve where $f_l = 0.5$. It is determined by the linear interpolation of the f_l field.

REFERENCES

[1] Bennon W.D., Incropera F.P., A continuum model for momentum, heat and species transport in binary solid–liquid phase change systems, Int. J. Heat Mass Tran. 30 (1987) 2161–2170.

[2] Patankar S.V., Numerical Heat Transfer and Fluid Flow, Hemisphere, New York, 1980.

[3] Mencinger J., Modeling of heat and momentum transport during melting and solidification, Master Thesis, University of Ljubljana, 1998.

APPENDIX X

Description of the algorithm used by:

Stéphane Couturier and Hamou Sadat*

LET UMR CNRS 6608, Ensma, 86960 Futuroscope cedex, France

Formulation of the equations

In a solid undergoing a solid-to-liquid phase transformation, the conservation of energy can be written in terms of the enthalpy h as:

$$\frac{\partial h}{\partial t}+\nabla\cdot(\boldsymbol{u}h)=\frac{1}{Ra^{1/2}}\nabla^2\theta \qquad (1)$$

where $\boldsymbol{u}$ is the velocity, h the enthalpy and $\theta = (T-T_F)/(T_H-T_F)$ the temperature in a dimensionless form. The reference quantities are the cavity height H, $\alpha Ra^{1/2}/H$ for velocity and related scales for time and pressure where α is the thermal diffusivity. The reference enthalpy is $\rho c\,(T_H - T_F)$, h is defined as:

$$h=\theta+\frac{g}{Ste} \qquad (2)$$

where g is the the volume fraction of liquid ($g = 1$ for $\theta > 0$ and $g = 0$ for $\theta = 0$).

In addition, using the Boussinesq approximation, the momentum and continuity equations that govern the laminar flow in the liquid phase can be written as:

$$\frac{\partial \mathbf{u}}{\partial t}+\mathbf{u}\cdot\nabla\mathbf{u}-\frac{Pr}{Ra^{1/2}}\nabla^2\mathbf{u}+\nabla p-\boldsymbol{S}=0 \qquad (3)$$

$$\nabla\cdot\mathbf{u}=0 \qquad (4)$$

where p is the pressure and $\boldsymbol{S}$ is a source term which takes the form:

$$\boldsymbol{S}=-C(1-g)\mathbf{u}+Pr\frac{\boldsymbol{g}}{||g||}\theta \qquad (5)$$

where C is the constant set to a large value (e.g., 1 010) and $\mathbf{g}$ is the acceleration due to the gravity. With the source term $\boldsymbol{S}$ and the formulation of the energy equation in terms of enthalpy, the governing equations are solved all over the domain without tracking the phase front.

Discretisation

Time discretisation

An implicit time discretisation is used with a constant time-step. The implicit discretisation of the energy equation involves a enthalpy–temperature relationship [1] to represent the non-linearity associated with the latent heat. The enthalpy is updated from the current temperature field via a truncated Taylor series expansion,

$$h^{n+1}=h^n+\left[\frac{\mathrm{d}h}{\mathrm{d}\theta}\right]_n\left(\theta^{n+1}-\theta^n\right) \qquad (6)$$

where the subscript $(n+1)$ refers to the iteration level. $\mathrm{d}h/\mathrm{d}\theta$ is determined with the $h-\theta$ curve which is related to equation (2). Note that at discontinuities in the $h-\theta$ curve, the slope $\mathrm{d}h/\mathrm{d}\theta$ can be accurately approximated using an arbitrarily large value (e.g., 10^8). The time discretisation of the energy equation is written as:

$$\frac{h^{n+1}-h^t}{\Delta t}+\nabla\cdot\left(\mathbf{u}^{n+1}h^{n+1}\right)=\frac{1}{Ra^{1/2}}\nabla^2\theta^{n+1} \qquad (7)$$

Finally, taking into account equations (6) and (7), we obtain:

$$\left[\frac{\mathrm{d}h}{\mathrm{d}\theta}\right]_n\frac{\theta^{n+1}}{\Delta t}-\frac{1}{Ra^{1/2}}\nabla^2\theta^{n+1}+\nabla\left(\mathbf{u}^{n+1}\left[\frac{\mathrm{d}h}{\mathrm{d}\theta}\right]_n\theta^{n+1}\right)=\frac{h^t}{\Delta t}-\nabla\left[\mathbf{u}^{n+1}\left(h^t-\left[\frac{\mathrm{d}h}{\mathrm{d}\theta}\right]_n\theta^n\right)\right] \qquad (8)$$

---

* sadat@let.ensma.fr

After the solution of equation (8), the $(n+1)$ enthalpy field is updated using equation (6). The local liquid fraction g is calculated from equation (2) with an over/undershoot correction that bounds g^{n+1} between 0 and 1.

Space discretisation

The linear algebraic equations are obtained using the diffuse approximation method [2, 3], a new numerical method for solving partial differential equations. This technique only requires sets of discretisation nodes. The equations are discretised on a uniformly spaced grid $N \times N$ in the solid phase and a mesh equivalent to a $2N \times 2N$ grid points in the liquid phase. The evolution of the mesh results of the evolution of the phase front: a remeshing occurs when the the liquid zone increases.

Solution of linear systems

The resulting linear systems are solved using the bi-conjugated gradient algorithm. The enthalpy, the momentum and the continuity equations are solved over all the computational domain. The continuity equation is replaced by a Poisson equation: this feature will be presented with the next part.

Incompressibility constraint

A projection method [4] is used for solving the momentum and continuity equations. Velocity and pressure are uncoupled and the equations are solved one after the other. The velocity field is determined by first calculating intermediate velocity values based on an estimated pressure distribution and then obtaining appropriate corrections to satisfy the continuity equation. First, equation (3) is linearised:

$$\frac{\mathbf{u}^* - \mathbf{u}^t}{\Delta t} + \mathbf{u}^n \cdot \nabla \mathbf{u}^* - \frac{Pr}{Ra^{1/2}} \nabla \mathbf{u}^* + \nabla p^n - S^n = 0 \quad (9)$$

where the subscript n indicates values known from the previous time step, t represents the previous time-step. We enforce continuity by writing:

$$\nabla^2 P' = -\frac{\nabla \mathbf{u}^*}{\Delta t} \quad (10)$$

Equation (10) is the Poisson equation for the pressure correction with homogeneous Neumann boundary conditions. Once the pressure correction p' has been determined, the corresponding velocity corrections are computed:

$$\mathbf{u}' = -\Delta t \, \nabla p' \quad (11)$$

Then,

$$\begin{aligned} \mathbf{u}^{n+1} &= \mathbf{u}^* + \mathbf{u}' \\ P^{n+1} &= P^n + P' \end{aligned} \quad (12)$$

Algorithm

(1) At the beginning of each time-step $(t + \Delta t)$, $[\,]^n = [\,]^t$ for scalar and velocity fields.

(2) Initial scalar and velocity fields are defined, $[\,]^n$.

(3) The momentum equations are solved to update the provisional velocity field, equation (9).

(4) The pressure correction equation is solved equation (10).

(5) The velocity corrections are calculated, equation (11).

(6) The pressure and velocity fields are updated, equation (12).

(7) The energy equation is solved equation (8), enthalpy and liquid fraction are updated.

(8) Steps 2–7 are repeated until convergence.

(9) Increment time-step.

Determination of the phase front

If $g = 1$, the grid point is considered as liquid and the interface is defined at the location between a liquid and a solid grid point ($g = 0$).

Computational parameters

The computations were performed with a dimensionless time-step $\Delta t = 0.5$ for cases 1 2 and $\Delta t = 0.05$ for case 3, respectively. Concerning the grid points, $N = 61$ for cases 1 and 3 and $N = 101$ for the second case. The discretisation space $N \times N$ is used in the solid phase, in the liquid phase the mesh size is equivalent to a spatial resolution $2N \times 2N$.

REFERENCES

[1] Swaminathan C.R., Voller V.R., On the enthalpy method, Int. J. Numer. Meth. Fl. 3 (1993) 223–244.

[2] Nayroles B., Touzot G., Villon P., L'approximation diffuse, C. R. Acad. Sci. Paris, Series II 313 (1991) 293–296.

[3] Prax C., Sadat H., Application of the diffuse approximation for solving fluid flow and heat transfer problems, Int. J. Heat Mass Tran. 39 (1996) 214–218.

[4] Comini G., Del Giudice S., Finite element solution of the incompressible Navier-Stokes equations, Numer. Heat Tr. 5 (1982) 463–478.